IMPERIAL

Engineering and Physical Sciences Research Council

ZEROAVIA

Propeller Wake Propagation within a Model Cooling Duct of a Hydrogen-Electric Aircraft

T. Bryce-Smith, O.R.H. Buxton, G. Papadakis, K. Steiros

Background
Motivation

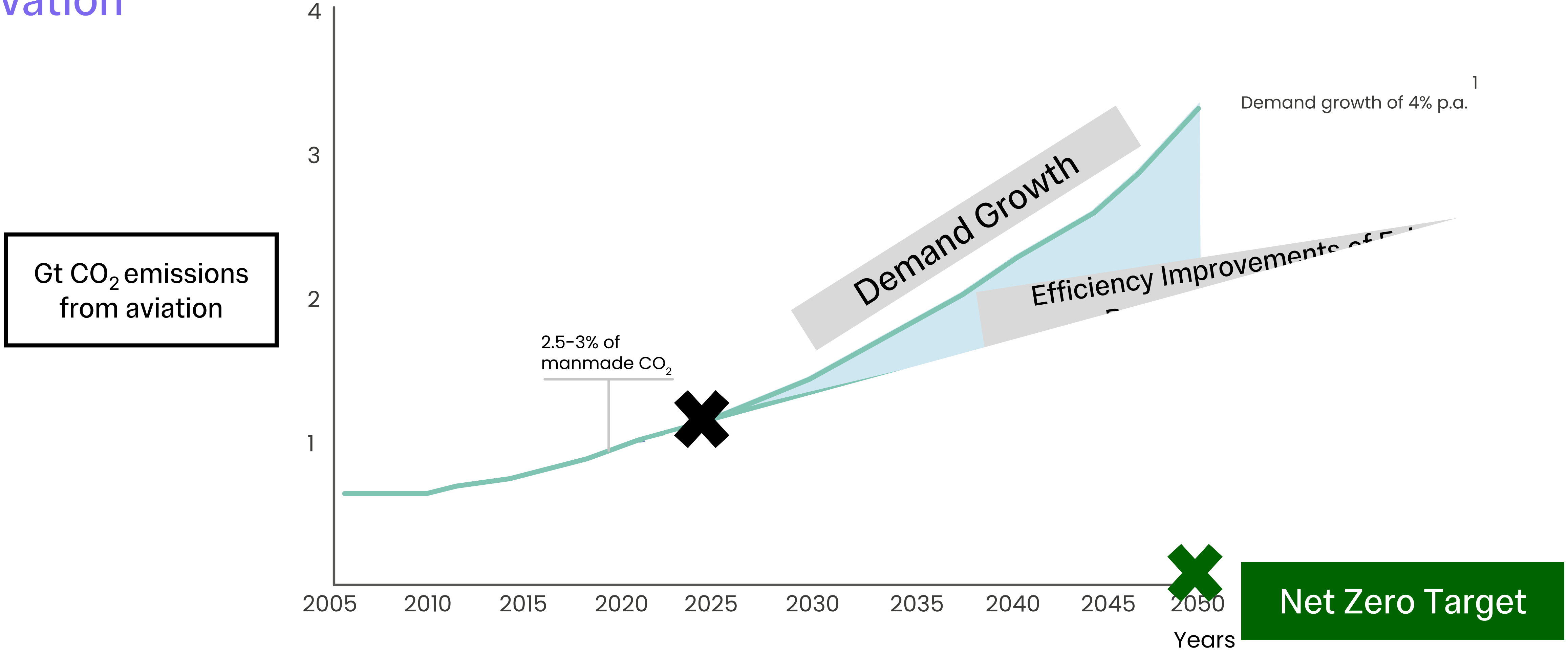

1. Assumption based on growth projections from ATAG, IATA, ICCT, WWF, UN
2. ICAO ambition incl. efficiency improvements in aircraft technology, operations and infrastructure

Source: *H_2ELIOS, 2023*

Background
Motivation

Hydrogen-based propulsion is here to stay in sustainable aviation

“… bon fue… **flight** f…

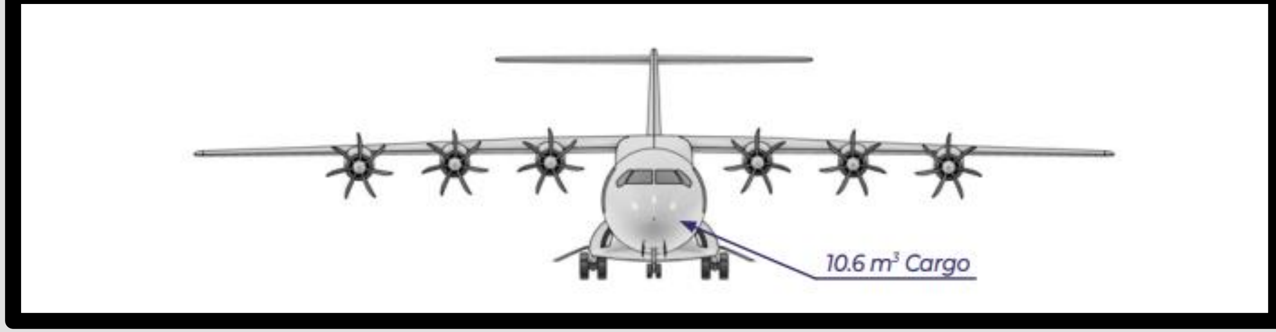

ATI, 2022. Design of a novel propeller regional aircraft.

ZeroAvia. Retrofit of current regional aircraft.

Thermal Management and Aerodynamic Structures for these aircraft require further study

“Thermal management will be a **key challenge for fuel cells.** The placement of this system has a **drag impact,** and the **weight of the system reduces the overall power density** of the fuel cell solution.”

FlyZero – Technology Roadmaps Report, ATI 2022

Background
The Challenge of Cooling Fuel Cells

Background

The Challenge of Cooling Fuel Cells

$$\dot{q} = h \cdot \Delta T$$

$\Delta T \approx 770°C$

$T_{\infty} \approx 30°C$

$T_{MAX} \approx 800°C$

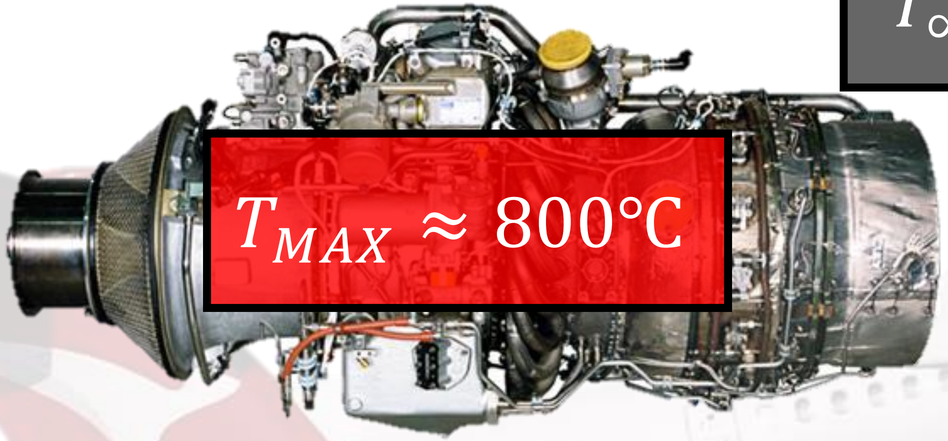

PW100: Conventional Turboprop Engine

Source: *Pratt & Whitney*

$\Delta T \approx 70 - 170°C$

$T_{MAX} \approx 100 - 200°C$

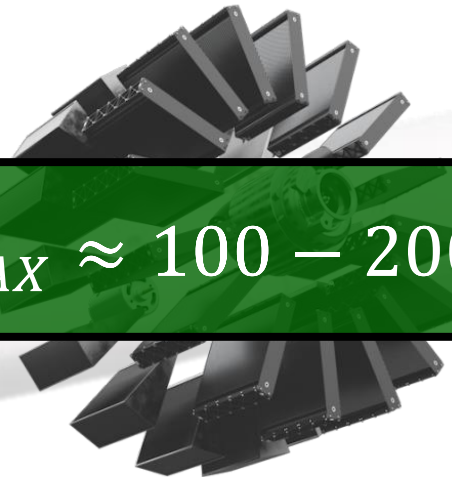

ZeroAvia's Proposed Aviation Fuel Cell

Background

The Challenge of Cooling Fuel Cells

$$\dot{q} = h \cdot \Delta T$$

$\Delta T \approx 770°C$

$\Delta T \approx 70 - 170°C$

More cooling air is required to cool a Fuel Cell, owing to reduced temperature gradients

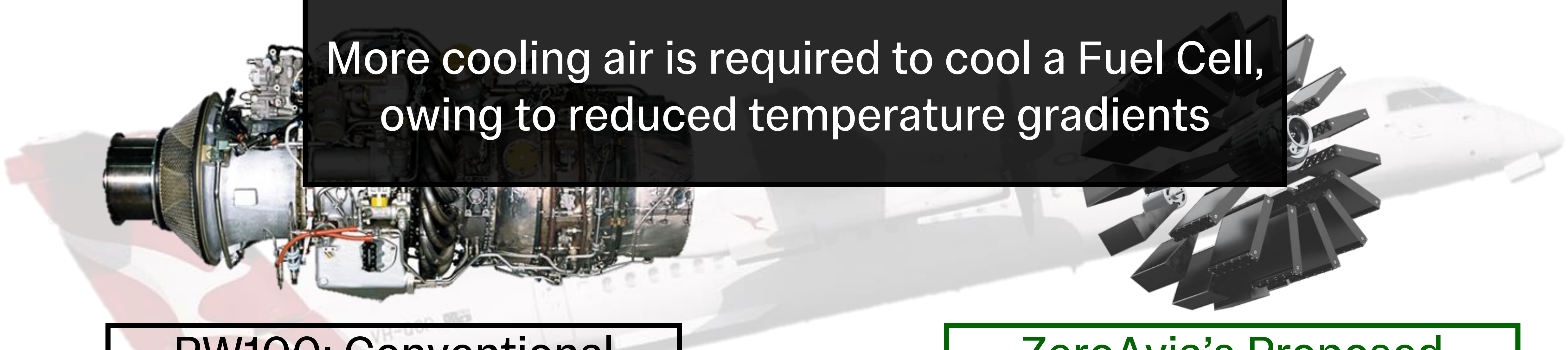

PW100: Conventional Turboprop Engine

ZeroAvia's Proposed Aviation Fuel Cell

Source: *Pratt & Whitney*

Background

Cooling in Hydrogen-Electric Aircraft

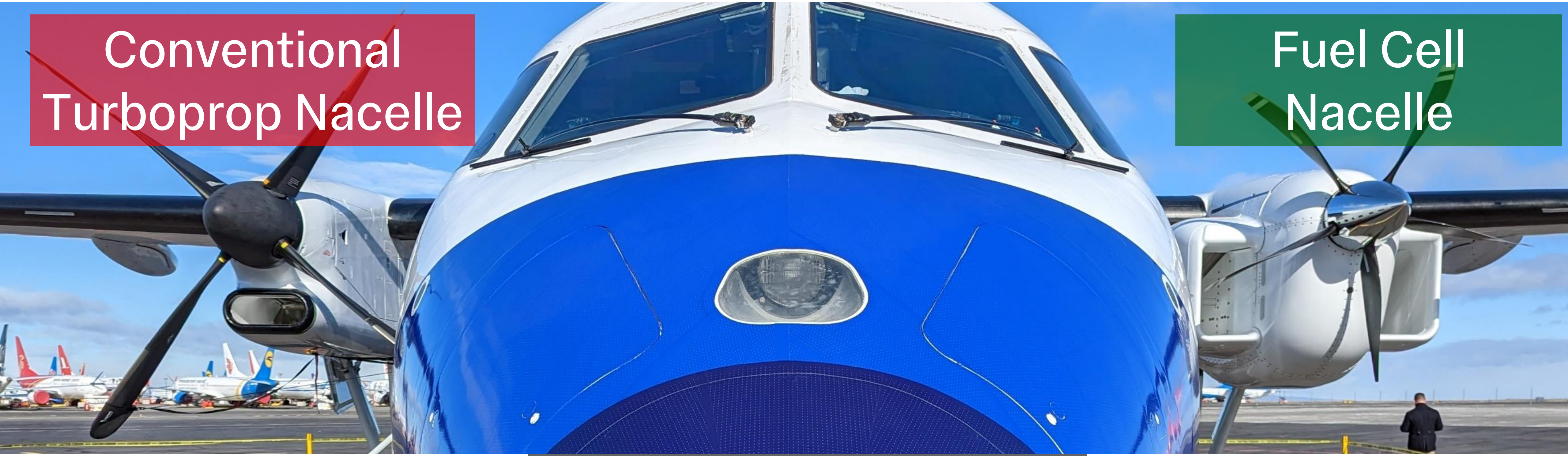

Universal Hydrogen's Fuel Cell Testbed

Background
Cooling in Hydrogen-Electric Aircraft

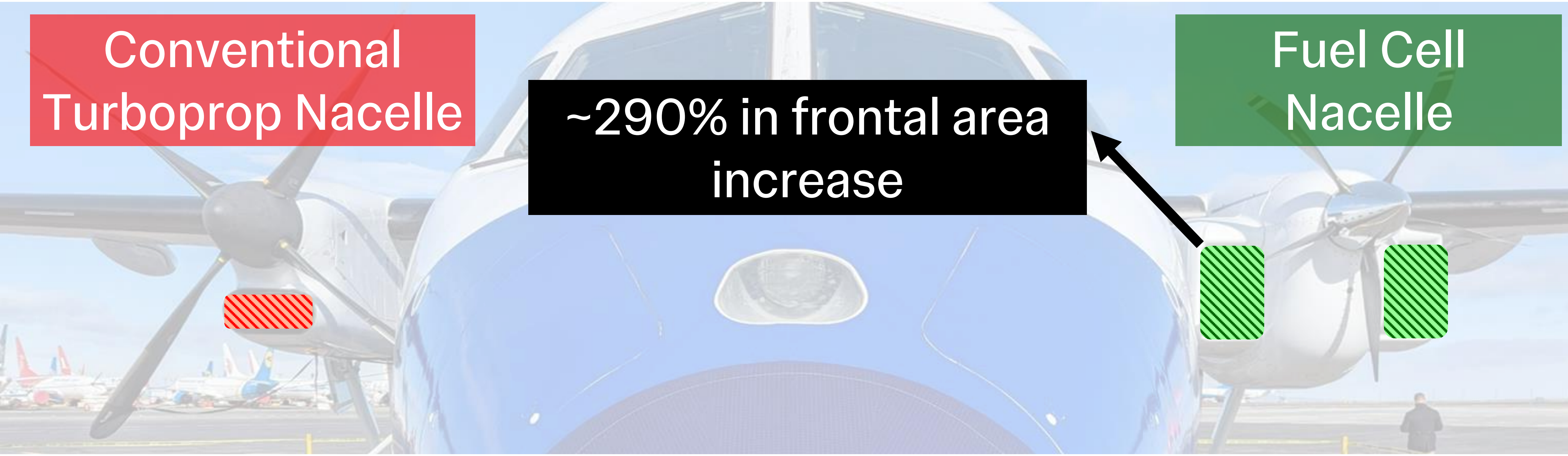

Source: *Universal Hydrogen*

Background
Research Questions

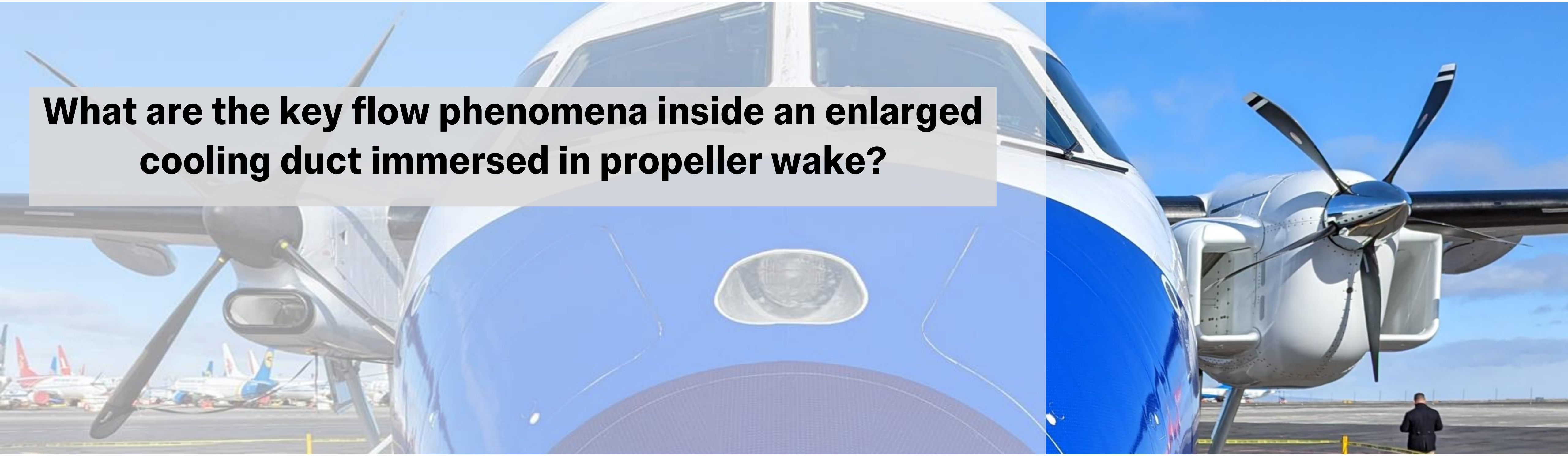

Background

Role of Unsteady Flow

Wakes from upstream rotor stages in turbomachines increase time-averaged laminar heat transfer by up to 60%

Park et al., 2014
ASME

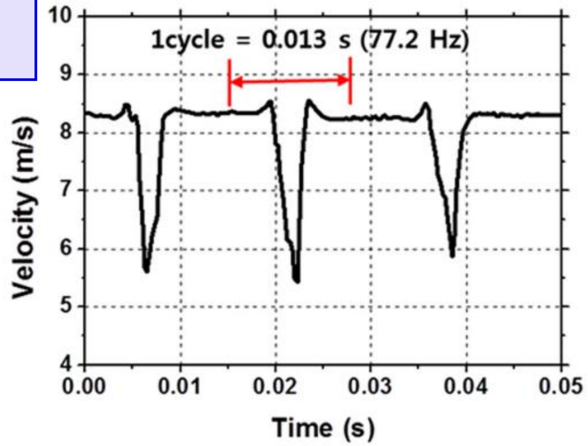

Doorly, 1988
J. Turbomachinery

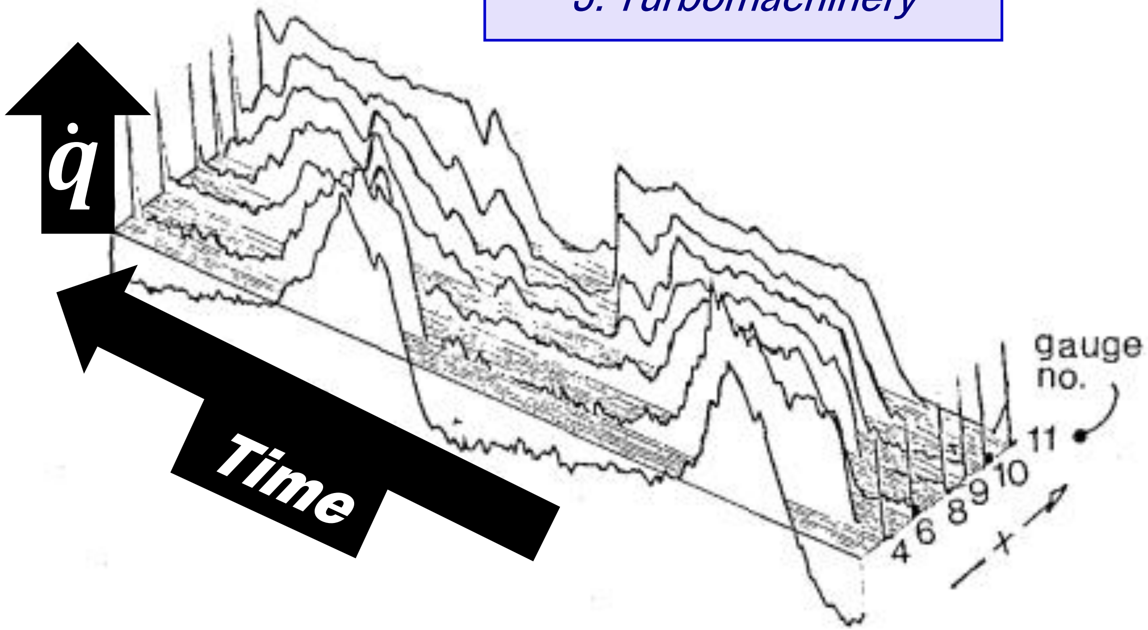

Background
Role of Unsteady Flow

Wakes from upstream rotor stages in turbomachines increase time-averaged laminar heat transfer by up to 60%

Park et al., 2014
ASME

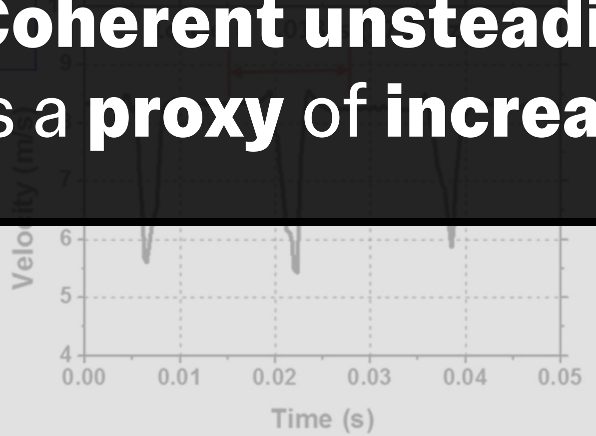

Doorly, 1988
J. Turbomachinery

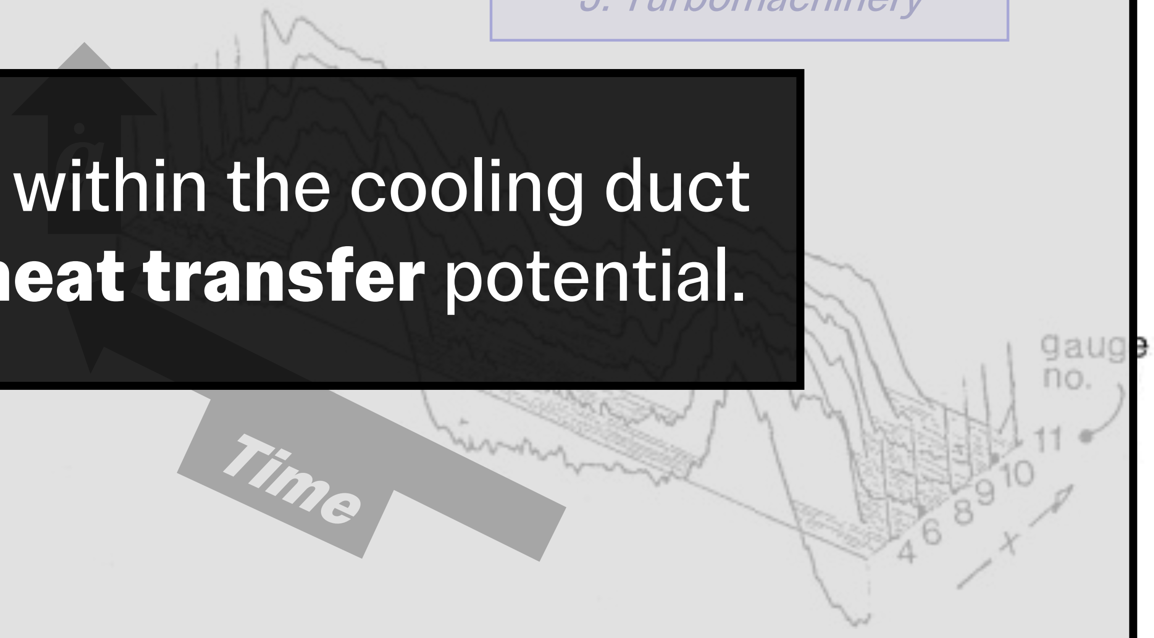

Coherent unsteadiness within the cooling duct is a **proxy** of **increased heat transfer** potential.

Background

Research Questions

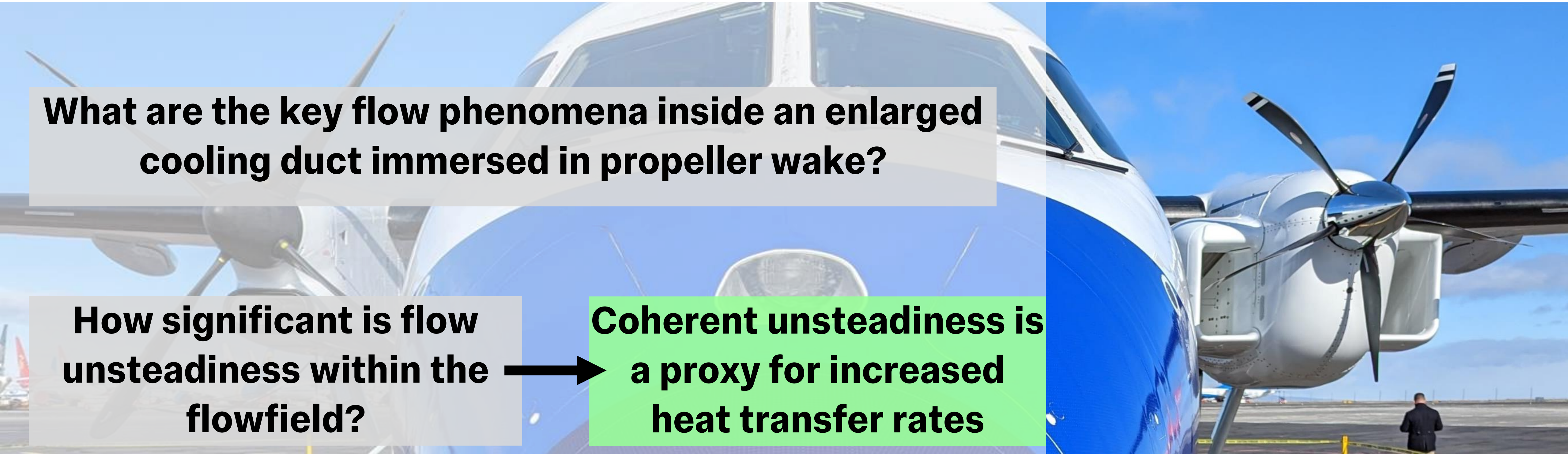

What are the key flow phenomena inside an enlarged cooling duct immersed in propeller wake?

How significant is flow unsteadiness within the flowfield? → **Coherent unsteadiness is a proxy for increased heat transfer rates**

How is the above affected by design and mission profile sensitive variables? → **Vary Advance Ratio, $J=V\infty/nD_D$, to capture changing flight condition**

Methodology
Prop and Duct

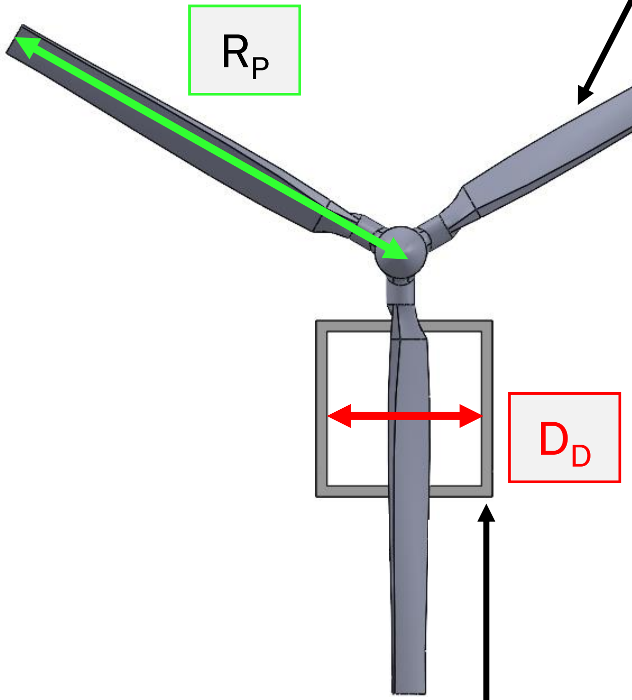

In-house propeller design
- **Fixed pitch**
- **Designed for J=1.18 (Climb Condition)**
- **Blockage of 14%**
- **Flat plate profile, 5% camber and 10% thickness**

Downstream square duct
- **Entirely transparent**
- **D_D/R_P ~ 40%**
- **Length ~ 41 D_D**

Advance Ratio, $J = V_\infty/nD_D$
Controlled by varying rotational speed, n

General		
Test Section Area:	600 x 600	mm
Propeller Radius, R_P:	127	mm
Propeller Chord:	10 - 20	mm
Duct Hydraulic Diameter, D_D:	44	mm
Duct Length, L_D:	1830	mm
Freestream Velocity, u_∞:	0.20	ms^{-1}
Chord Reynolds Number, Re_c:	7000	
Duct Reynolds Number, Re_D:	8400	

Methodology
Prop and Duct

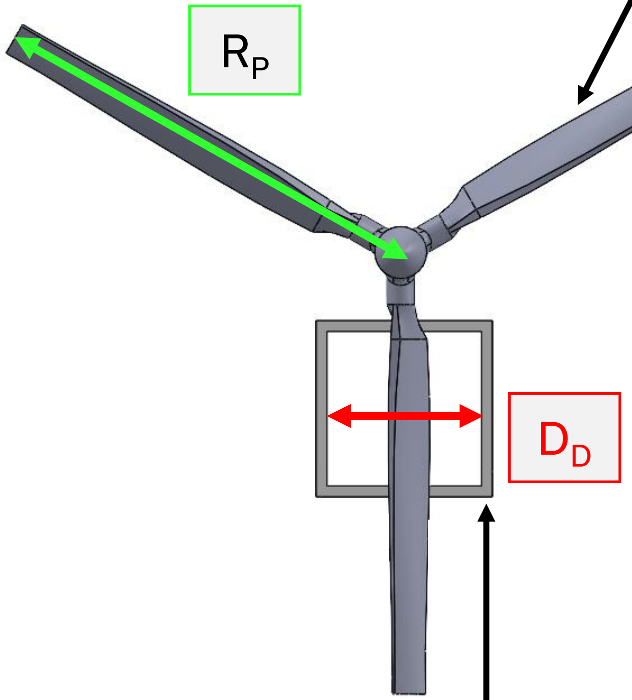

In-house propeller design
- **Fixed pitch**
- **Designed for J=1.18 (Climb Condition)**
- **Blockage of 14%**
- **Flat plate profile, 5% camber and 10% thickness**

Downstream square duct
- **Entirely transparent**
- **D_D/R_P ~ 40%**
- **Length ~ 41 D_D**

Advance Ratio, $J = V_\infty/nD_D$
Controlled by varying rotational speed, n

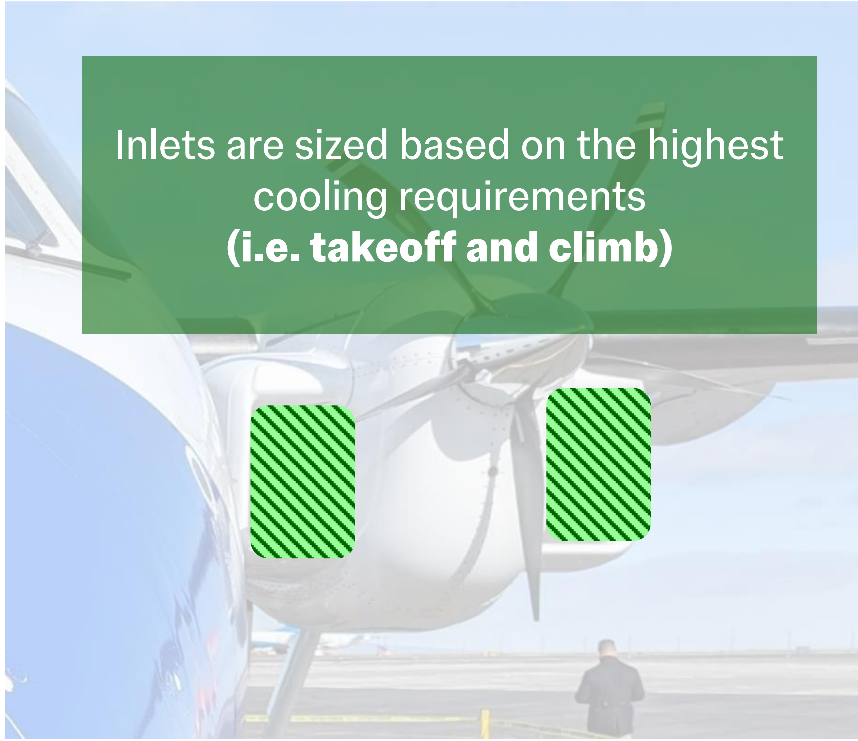

General		
Test Section Area:	600 x 600	mm
Propeller Radius, R_P:	127	mm
Propeller Chord:	10 - 20	mm
Duct Hydraulic Diameter, D_D:	44	mm
Duct Length, L_D:	1830	mm
Freestream Velocity, u_∞:	0.20	ms^{-1}
Chord Reynolds Number, Re_c:	7000	
Duct Reynolds Number, Re_D:	8400	

Methodology

Fixing the Prop and Duct

Propeller attached to rotor rig

- **Top traverse to move field of view**
- **Driven by stepper motor via vertical pulley**
- **Biswas and Buxton (2024)**

Duct held by low profile aluminum rig

- **Inlet 1D_D downstream of propeller**
- **<2% blockage**
- **No visible vibration**
- **Holds pipe**

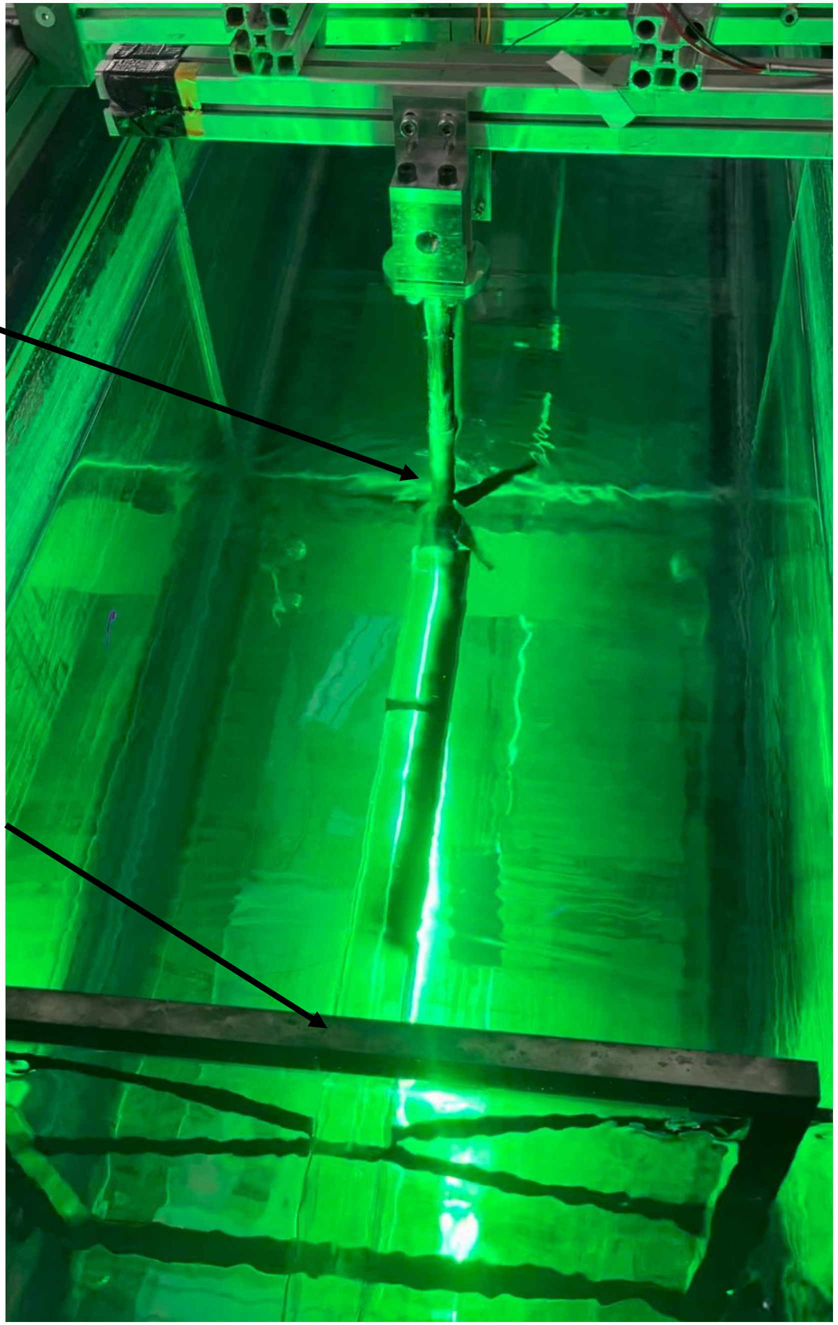

Hydrodynamics Flume

Methodology

PIV Setup

Single Phantom v641 Camera

- **Cinematographic mode**
- **f_{aq} = 100Hz**
- **Perpendicular to duct wall**

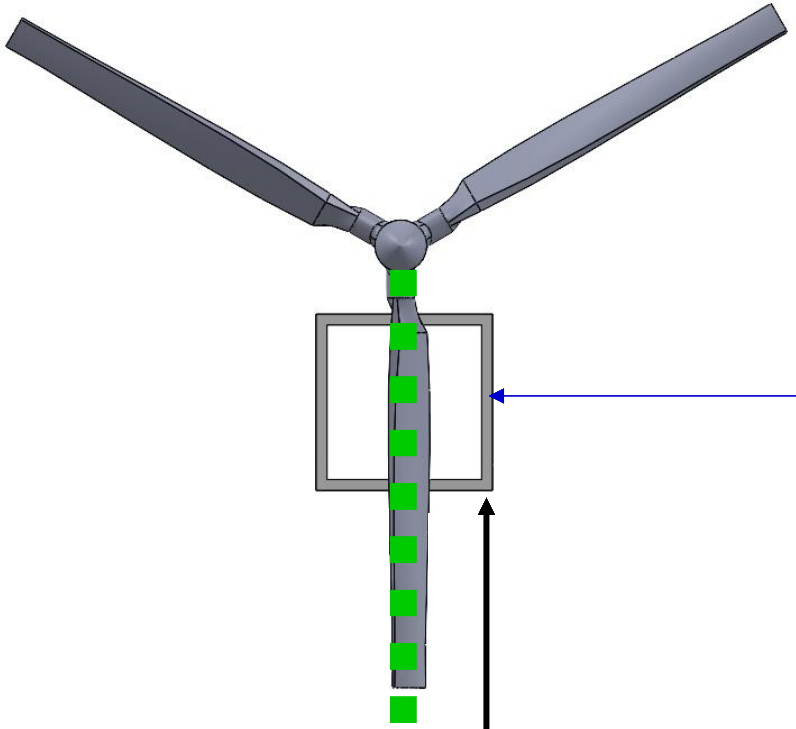

Planar PIV Setup

- **Sheet aligned with pipe midplane**
- **Water seeded with glass spheres**

PIV	
Seeding:	Water seeded with 9–12μm hollow glass spheres
Laser:	Nd:YLF, 527nm wavelength
Camera:	1x Phantom v641, Nikon AF NIKKOR 50mm f/1.4D
Capture:	Cinematographic mode, 100Hz acquisition frequency
Analysis:	Multi-pass, Final pass: 32 px × 32 px, 50% Overlap
Spatial Resolution:	2.3mm

Methodology

PIV

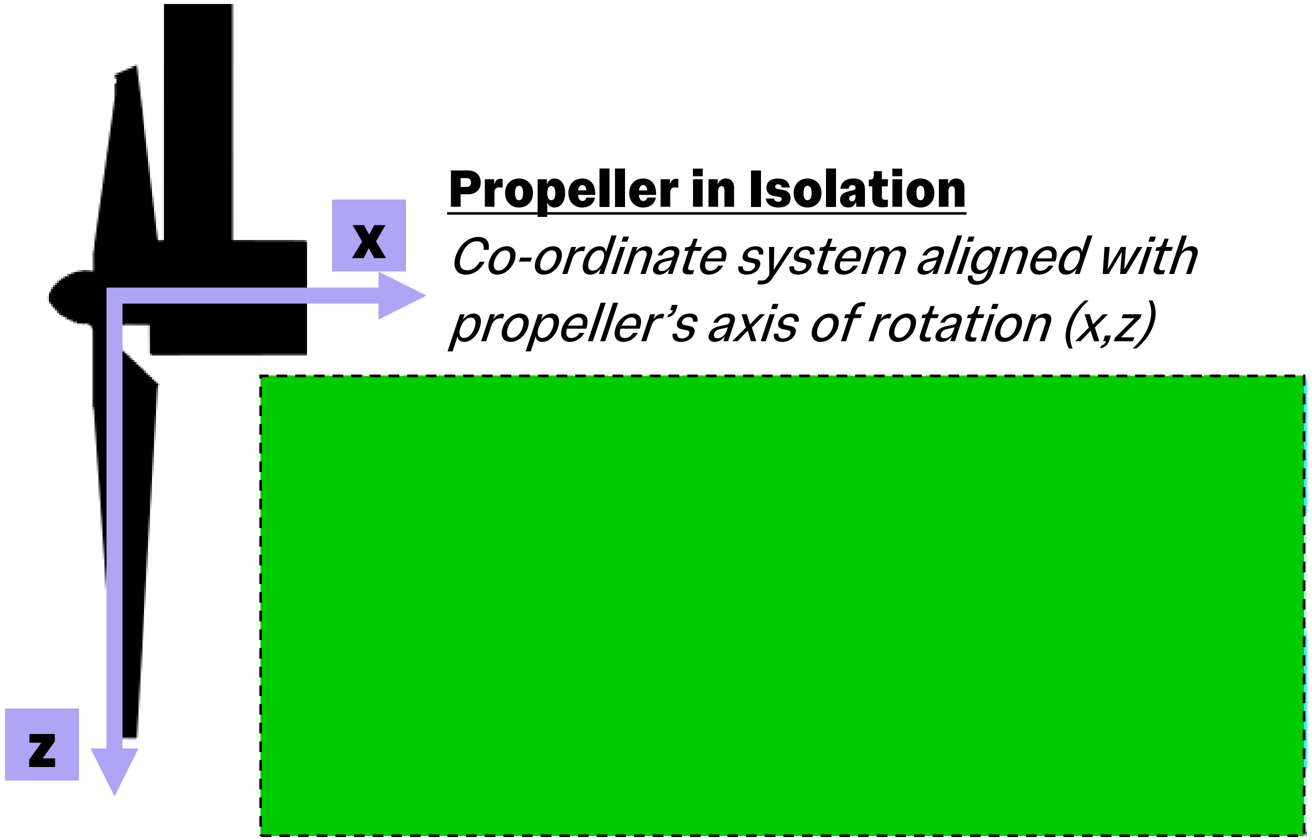

<u>Propeller in Isolation</u>

Co-ordinate system aligned with propeller's axis of rotation (x,z)

Results - Characterising the Propeller in Isolation
Summary

The propeller produces a characteristic wake, as compared to literature by:

1. The formation of **three discrete vortical structures** that undergo expected magnitude changes and transition downstream with changing advance ratio. [Ahmed et. al (2020)]

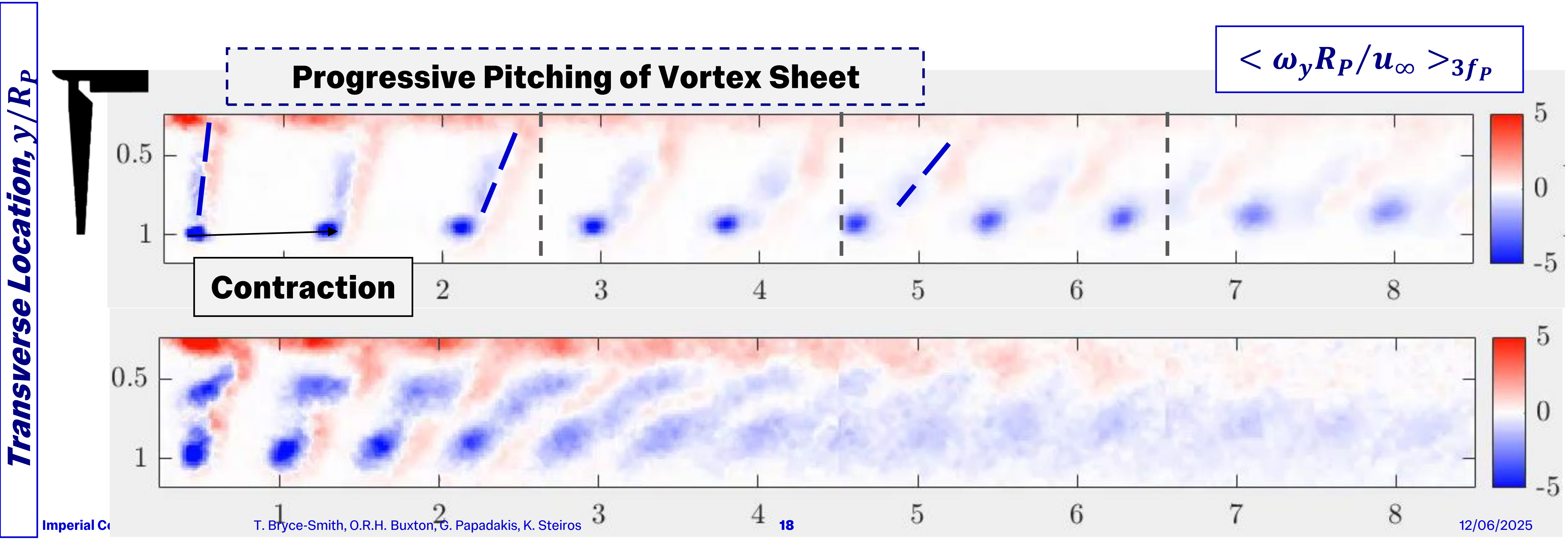

Results - Characterising the Propeller in Isolation
Summary

The propeller produces a characteristic wake, as compared to literature by:

2. An expected **two-step energy transfer** associated with evolution of coherent unsteadiness in three-bladed rotor wakes [Felli (2011), Biswas and Buxton (2024)]

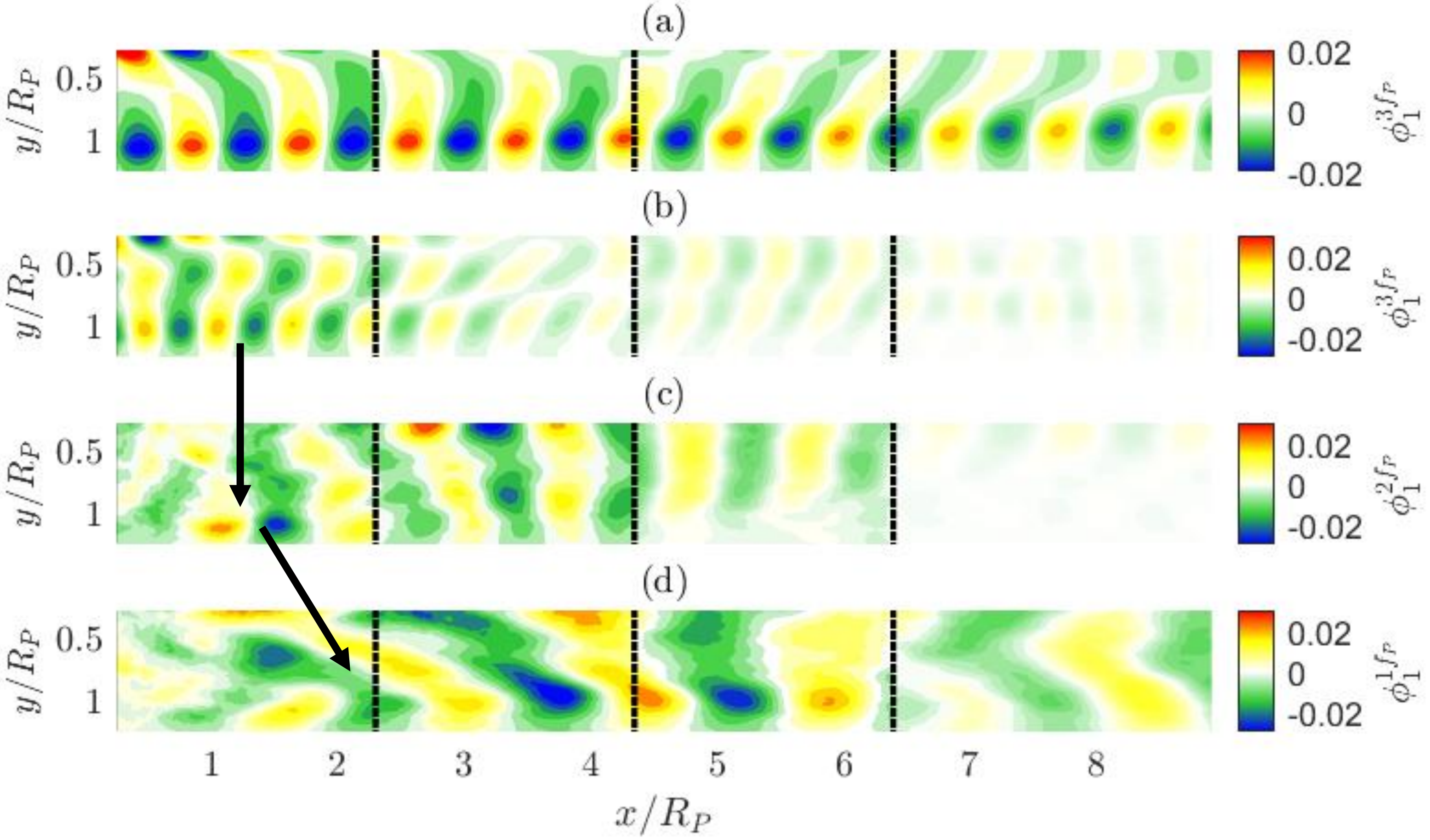

Results - Characterising the Propeller in Isolation
Summary

The propeller produces a characteristic wake, as compared to literature by:

1. The formation of **three discrete vortical structures** that undergo expected magnitude changes and transition downstream with changing advance ratio. [Ahmed et. al (2020)]
2. An expected **two-step energy transfer** associated with evolution of coherent unsteadiness in three-bladed rotor wakes [Felli (2011), Biswas and Buxton (2024)]

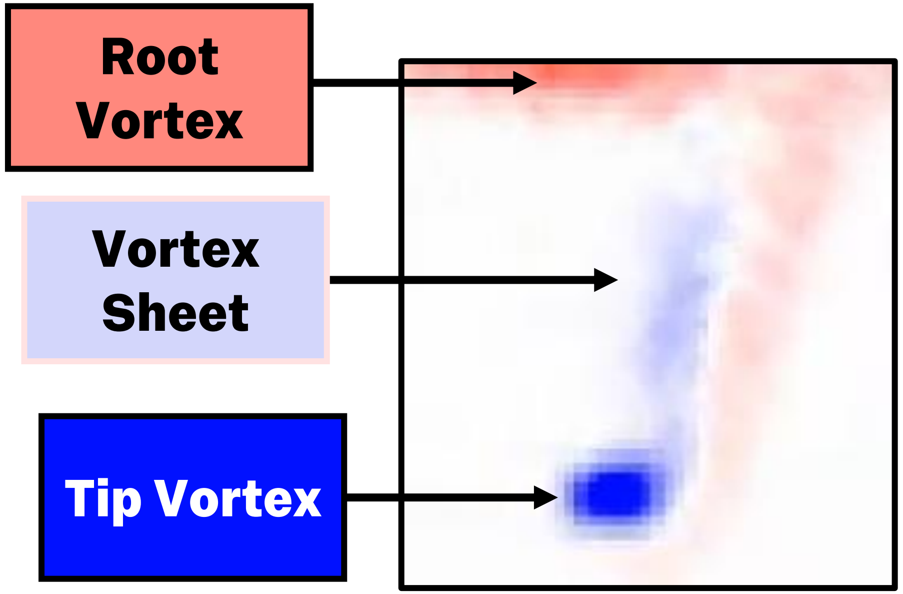

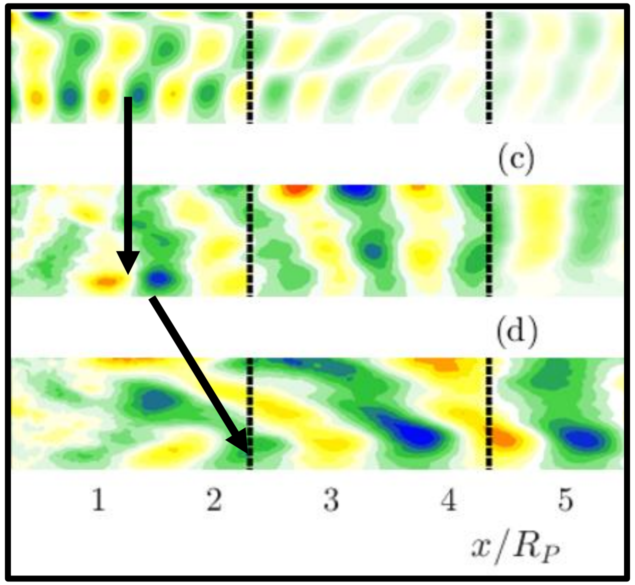

Methodology

PIV

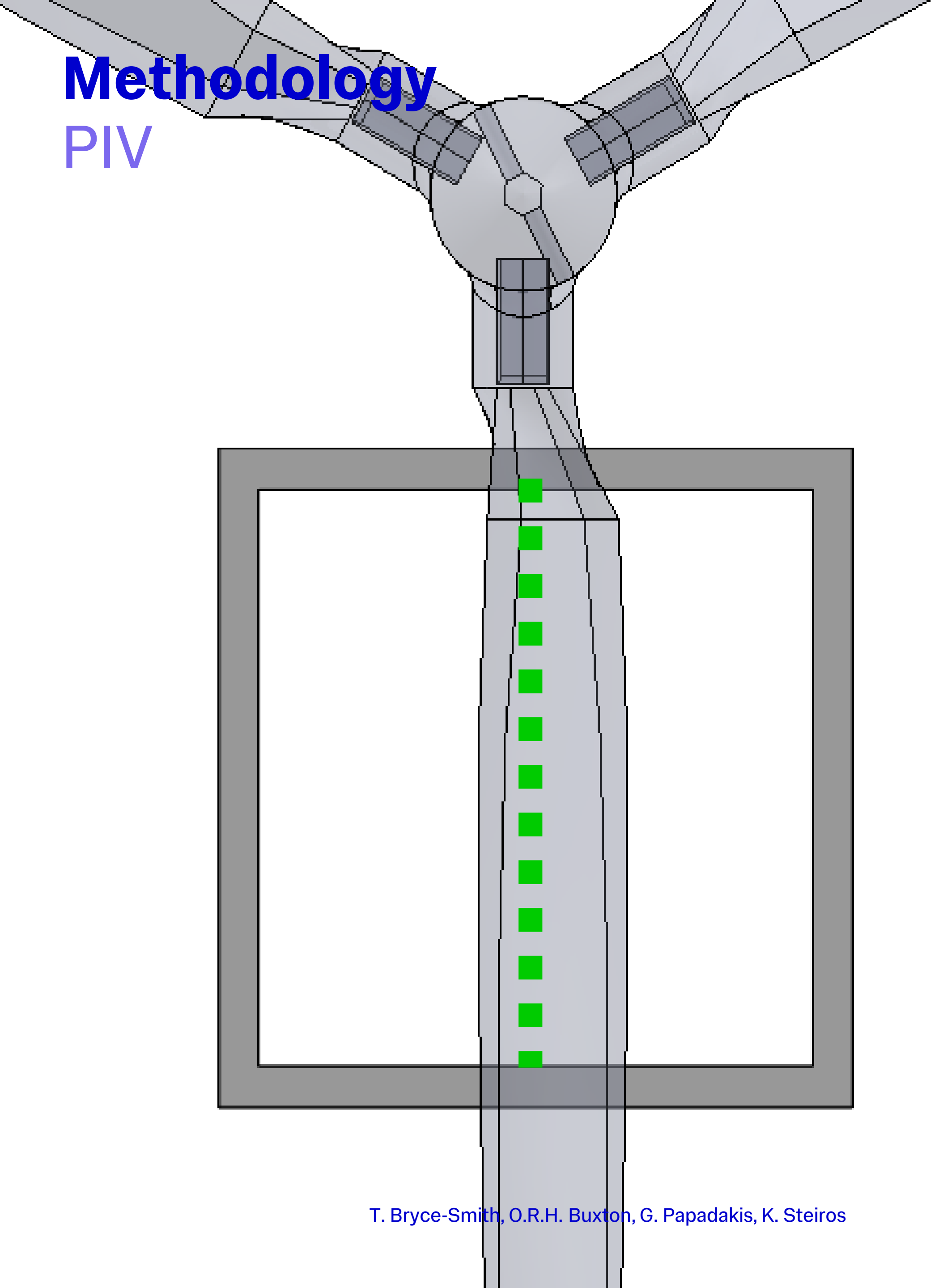

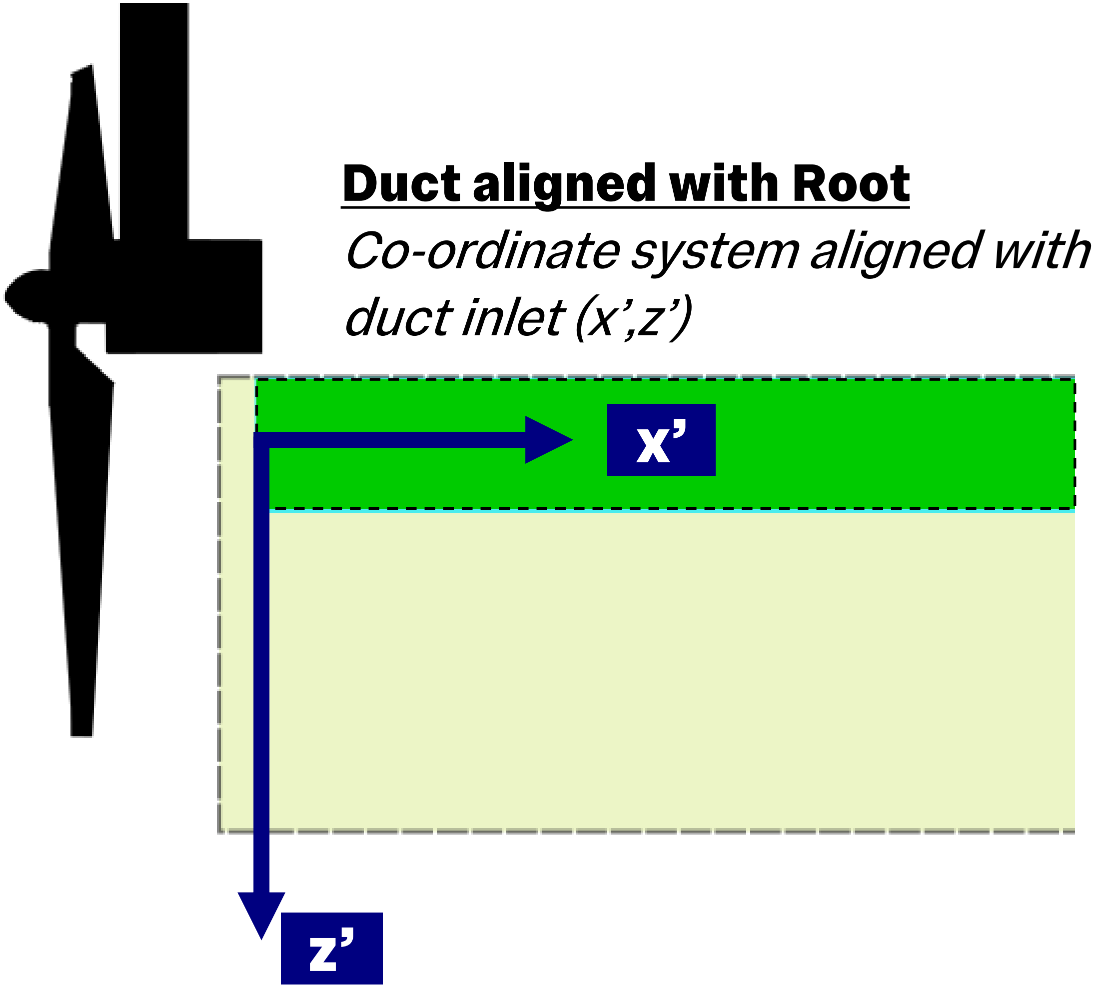

<u>Duct aligned with Root</u>

Co-ordinate system aligned with duct inlet (x’,z’)

Results – Duct in Root Position

Design Rotational Speed, J = 1.18

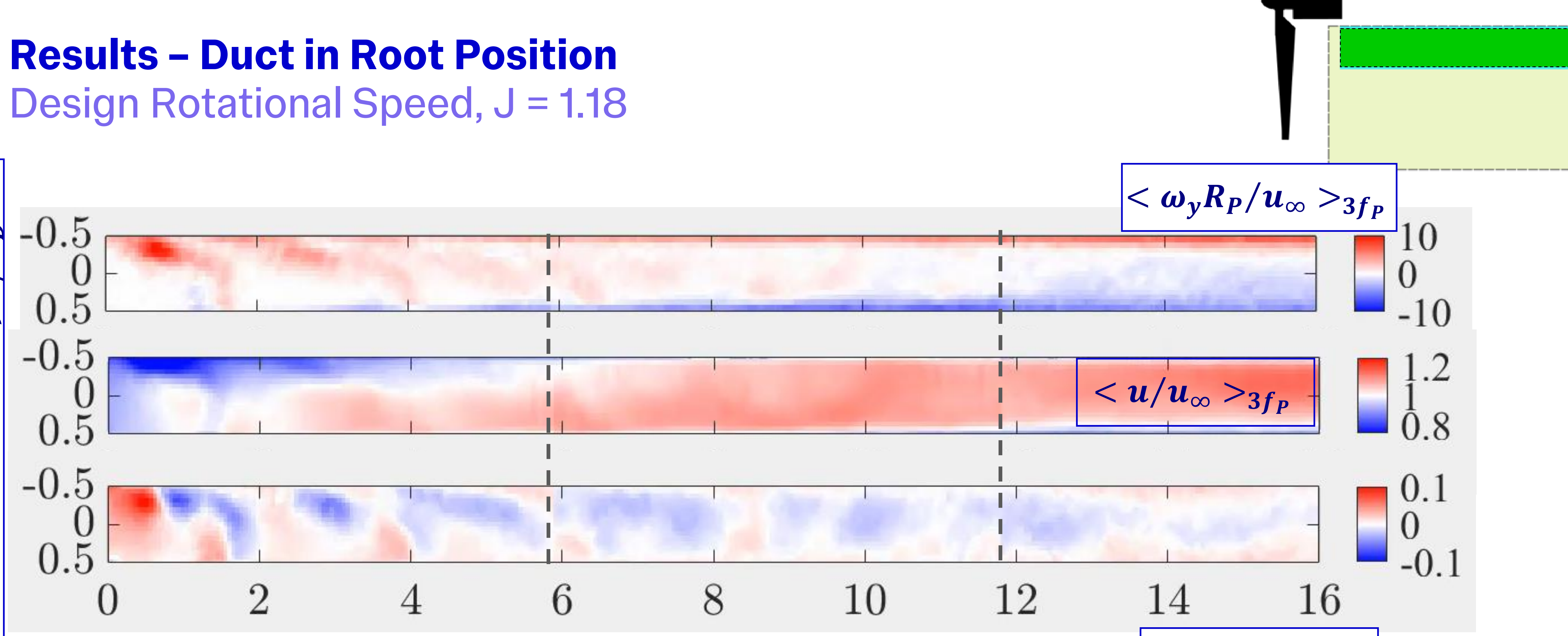

Transverse Location, z'/D_D

Streamwise Location, x'/D_D

Results – Duct in Root Position

Design Rotational Speed, J = 1.18

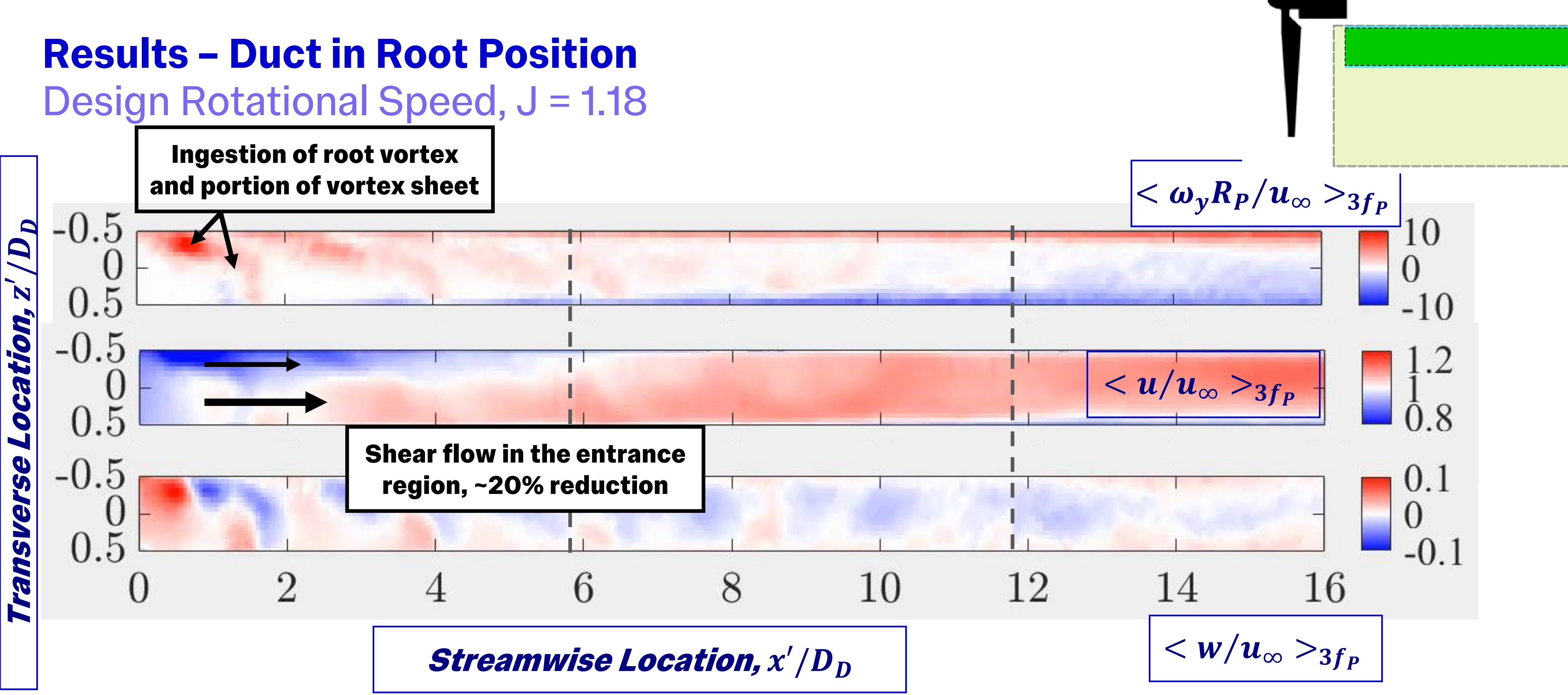

Results – Duct in Root Position

Design Rotational Speed, J = 1.18

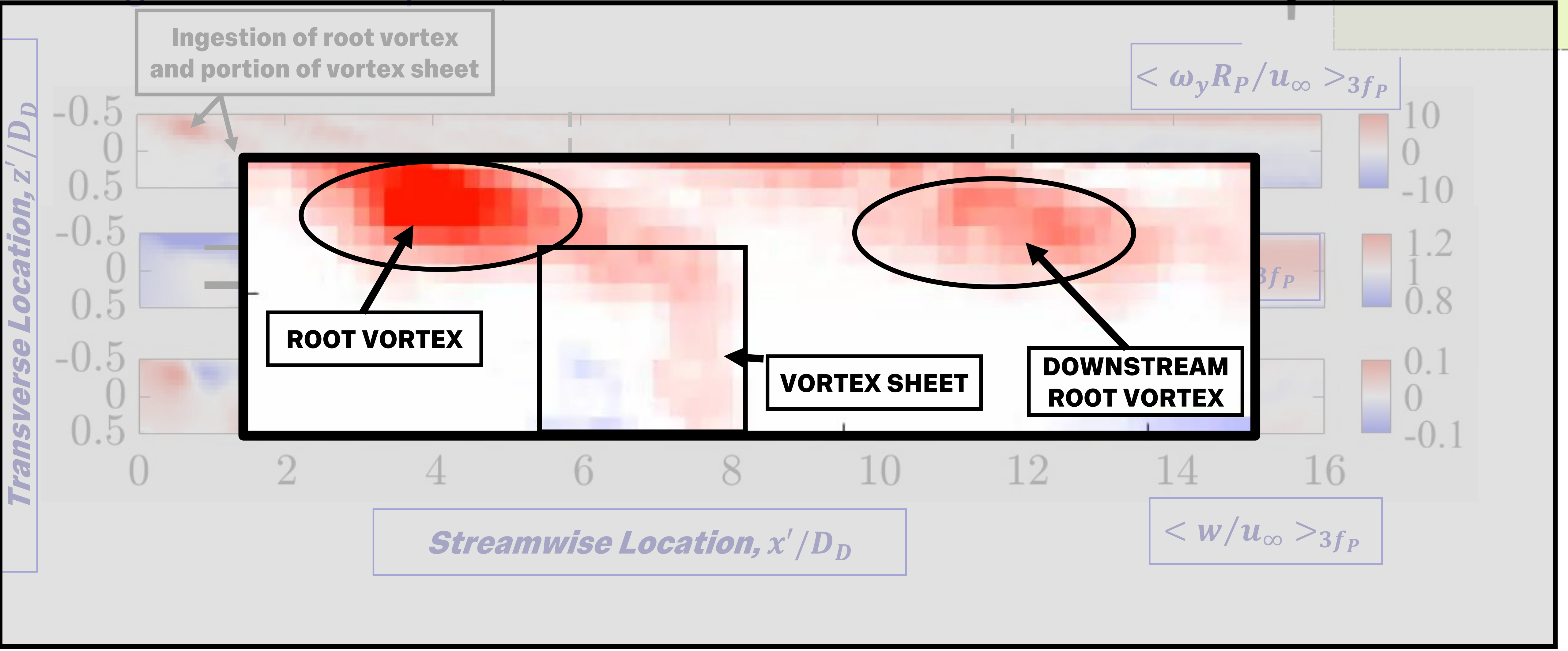

Results – Duct in Root Position

High Rotational Speed, J = 0.78

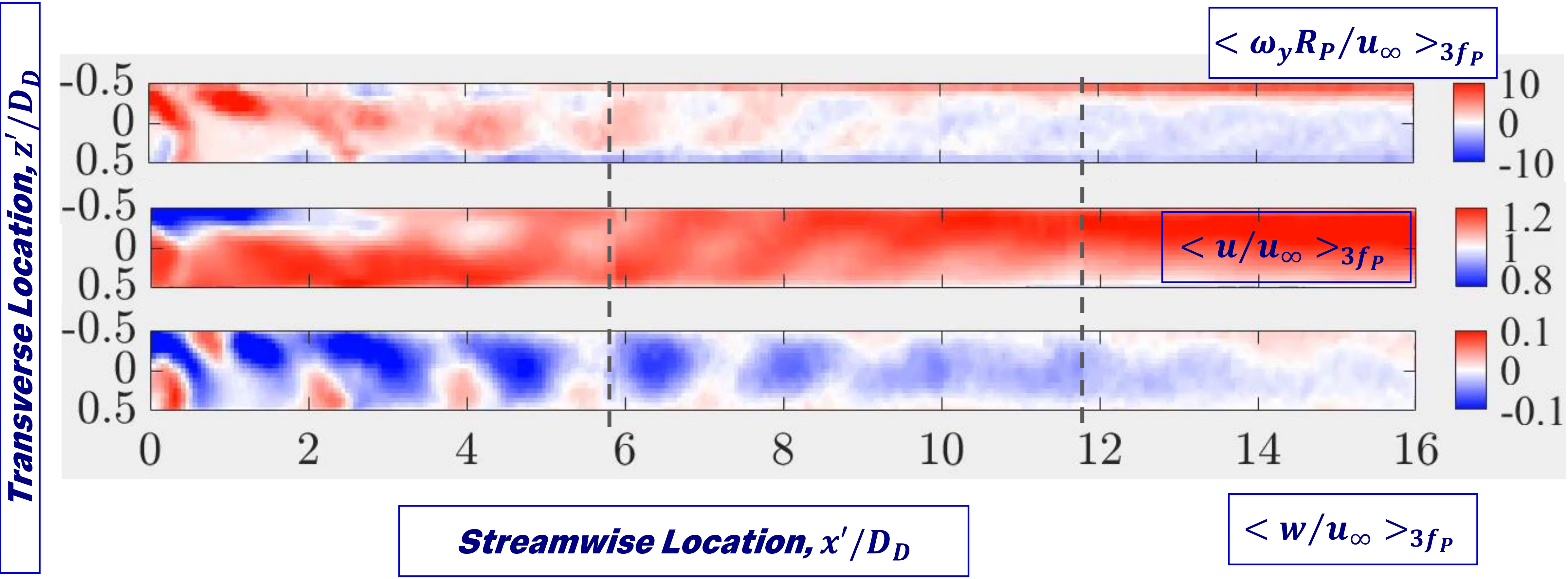

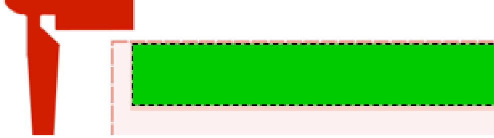

Results – Duct in Root Position

High Rotational Speed, J = 0.78

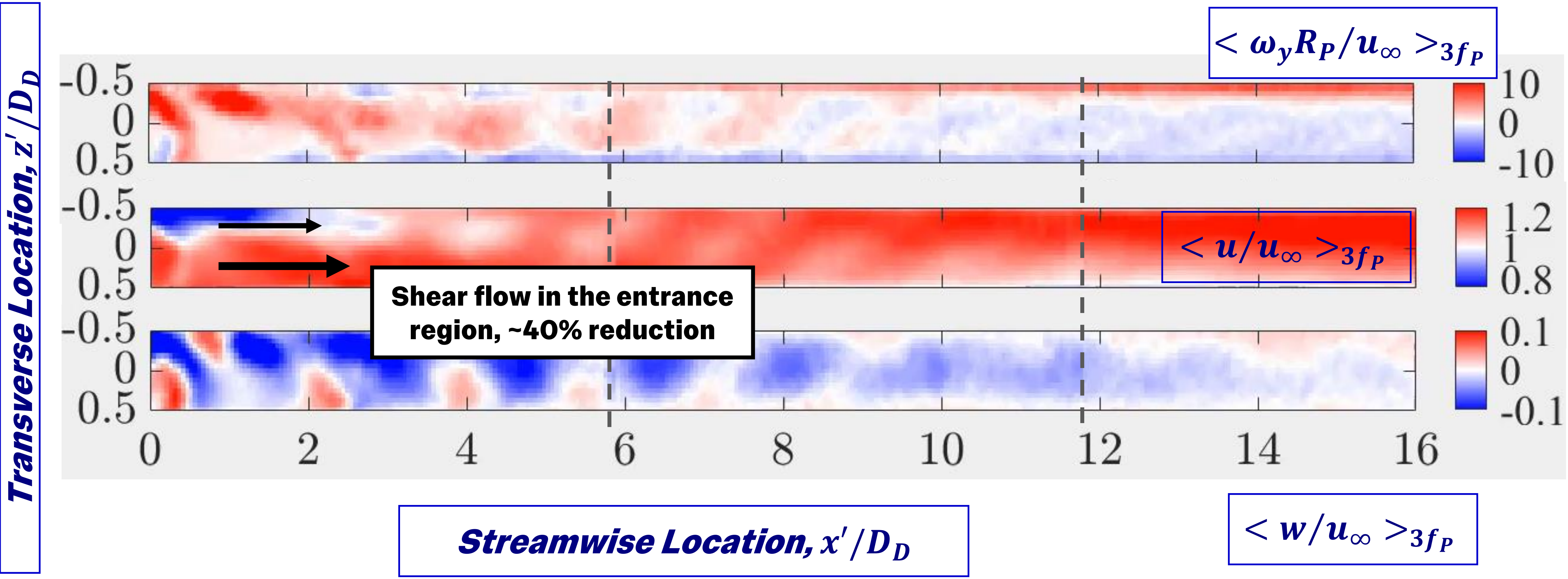

Results – Duct in Root Position

High Rotational Speed, J = 0.78

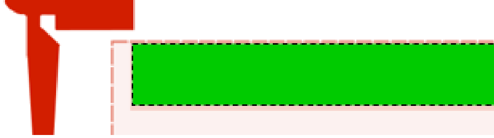

$< \omega_y R_P / u_\infty >_{3f_P}$

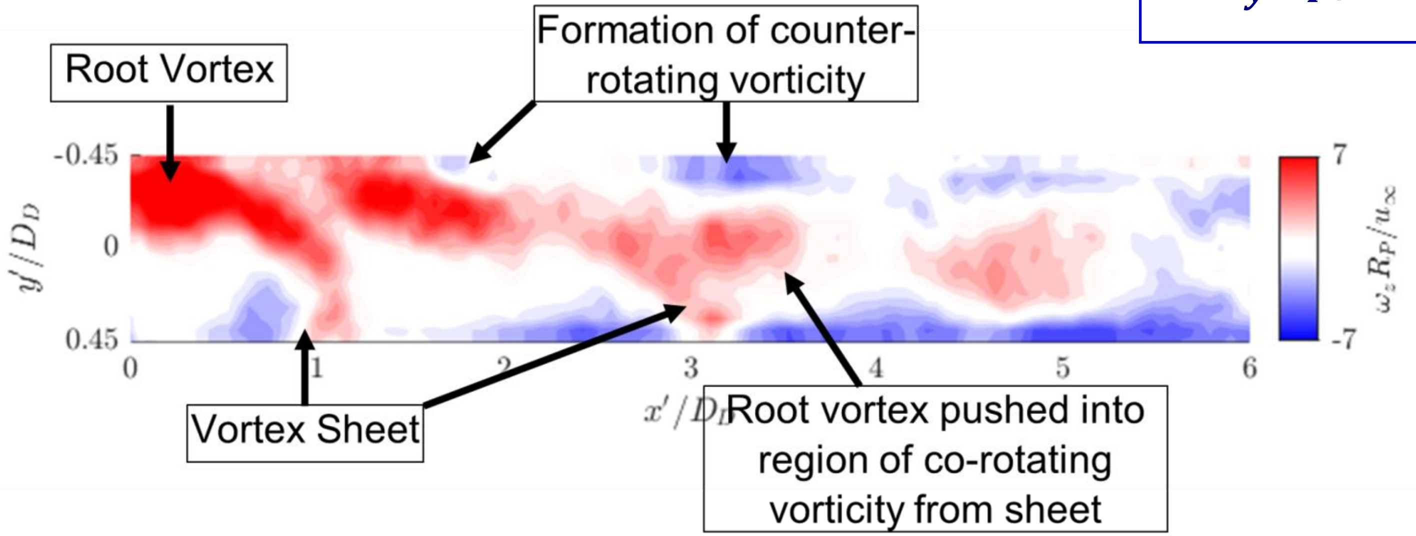

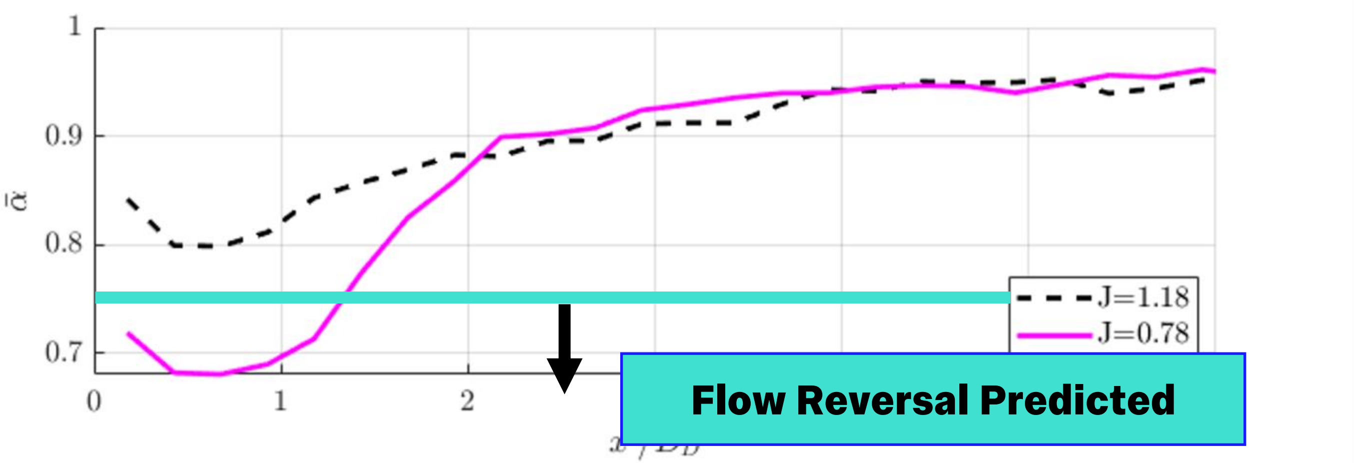

Doligalski and Walker (1984)

$$\alpha = 1 + \frac{u_{ind}}{u_\infty}$$

$$u_{ind} = \Gamma / 4\pi\varepsilon$$

Where:

- ε = distance from core to the wall
- Γ = circulation of root vortex

Results – Duct in Root Position
High Rotational Speed, J = 0.78

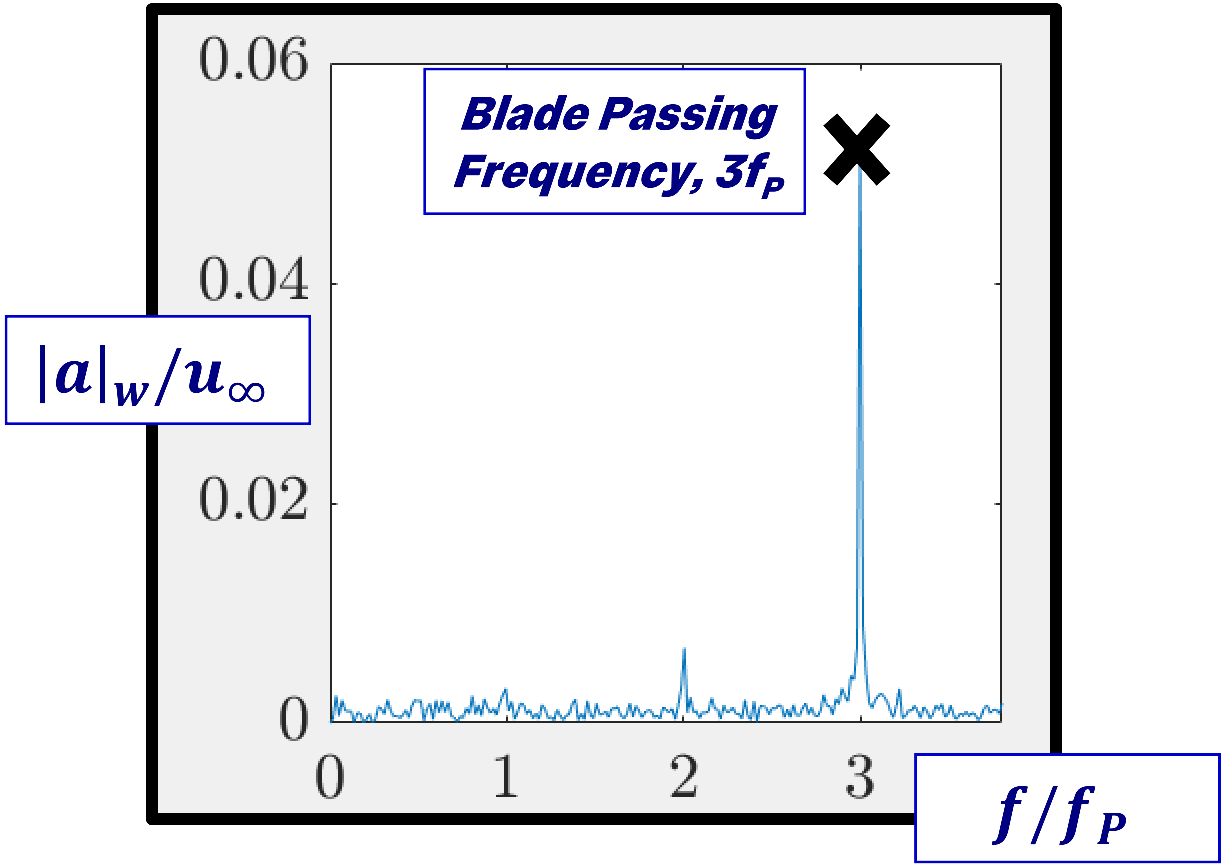

Results – Duct in Root Position

Changing Advance Ratio

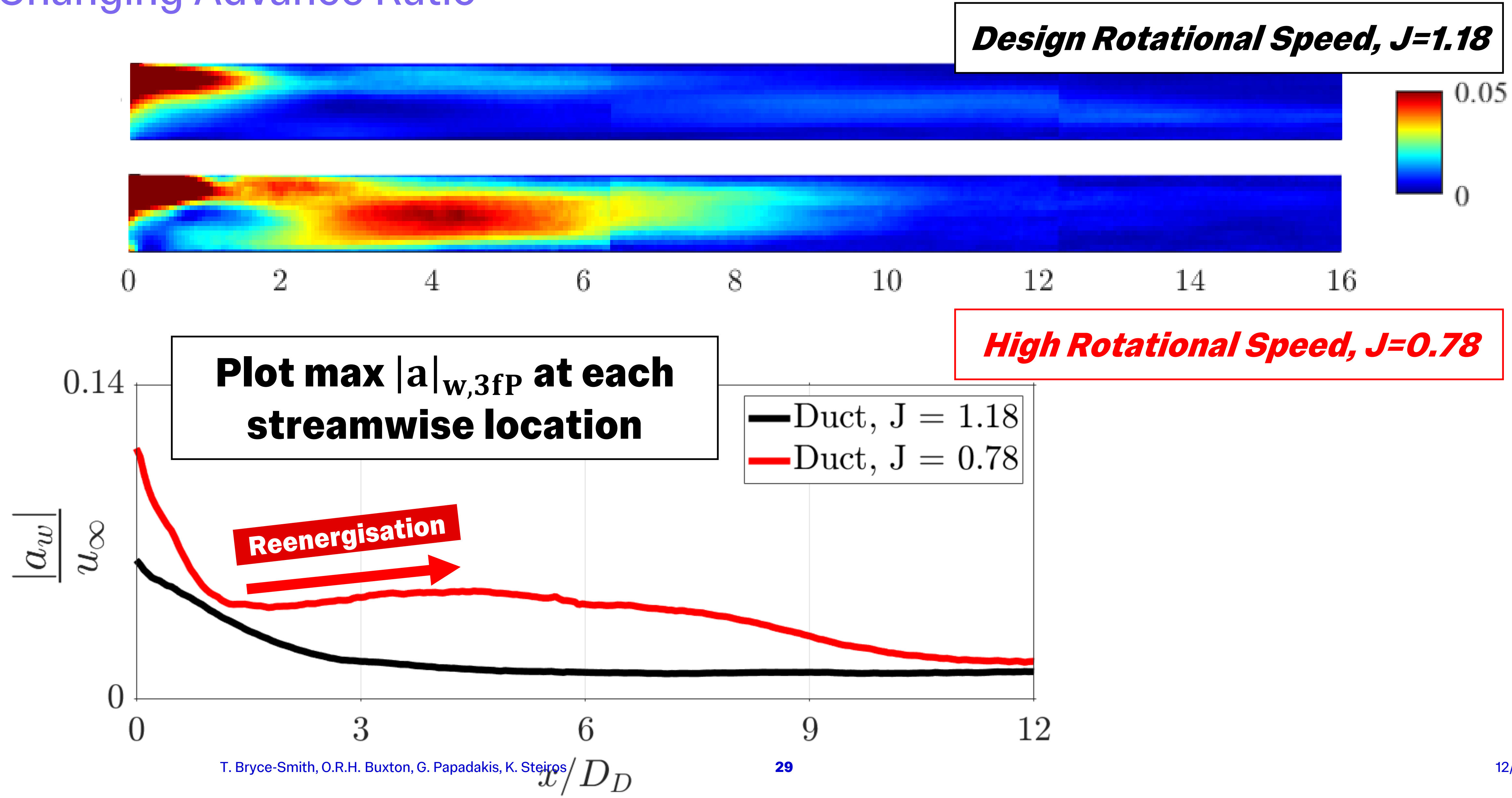

Results – Duct in Root Position

Changing Advance Ratio

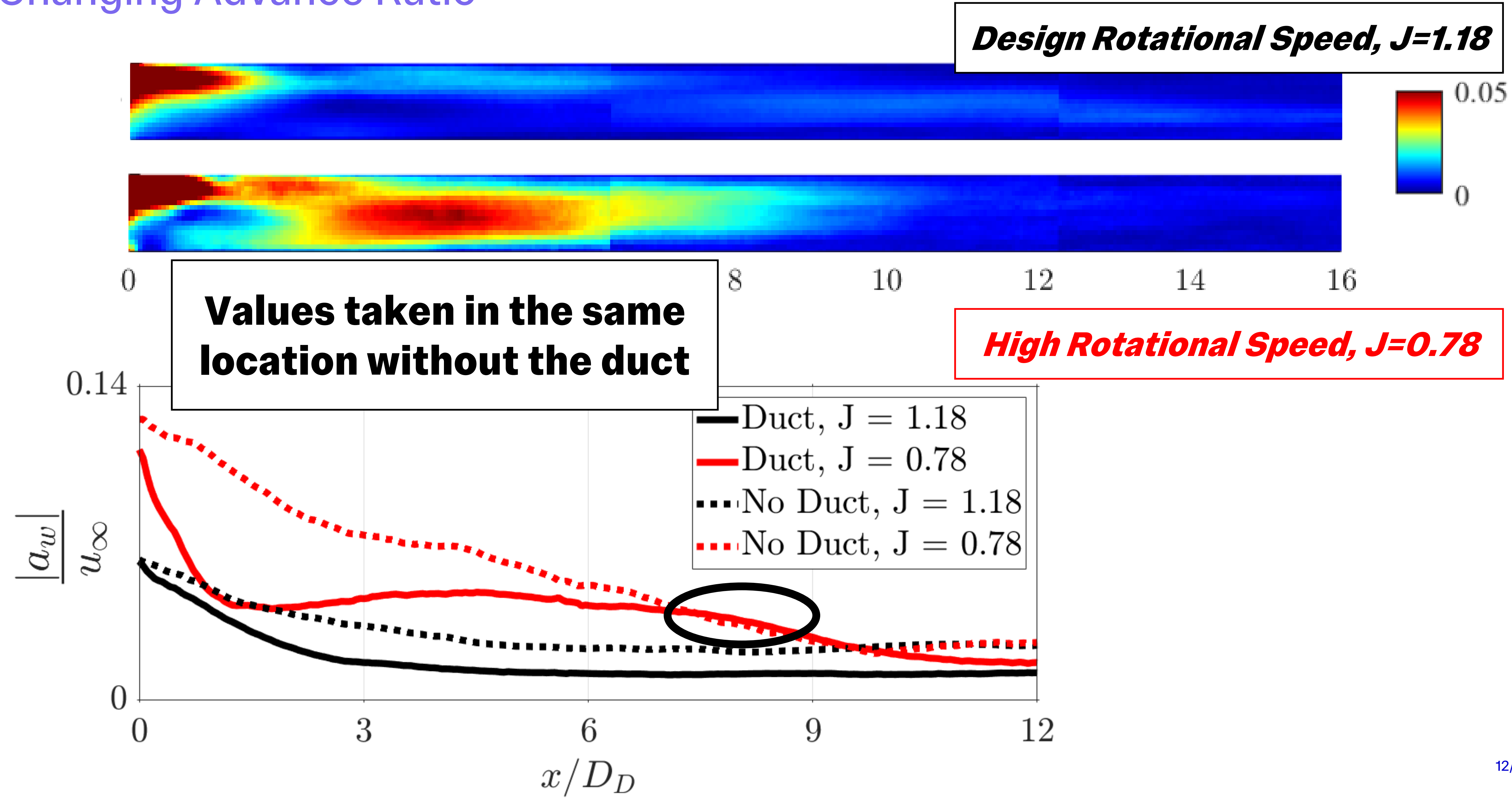

Summary of Findings

The root vortex and vortex sheet enter the duct.

The root vortex dominates the mean flowfield and turbulence statistics

The root vortex undergoes vortex-induced separation when at sufficient strength

Energies at 3fP are re-energized when this occurs and the locus moves to the centre of the duct

These decay into incoherent frequencies, rather than 2fP and 1fP when in isolation

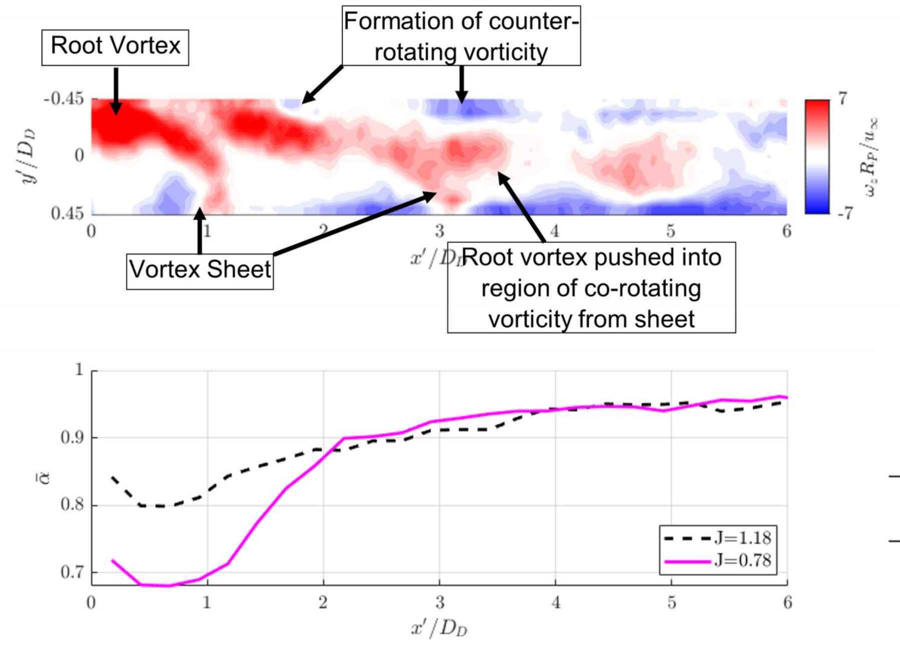

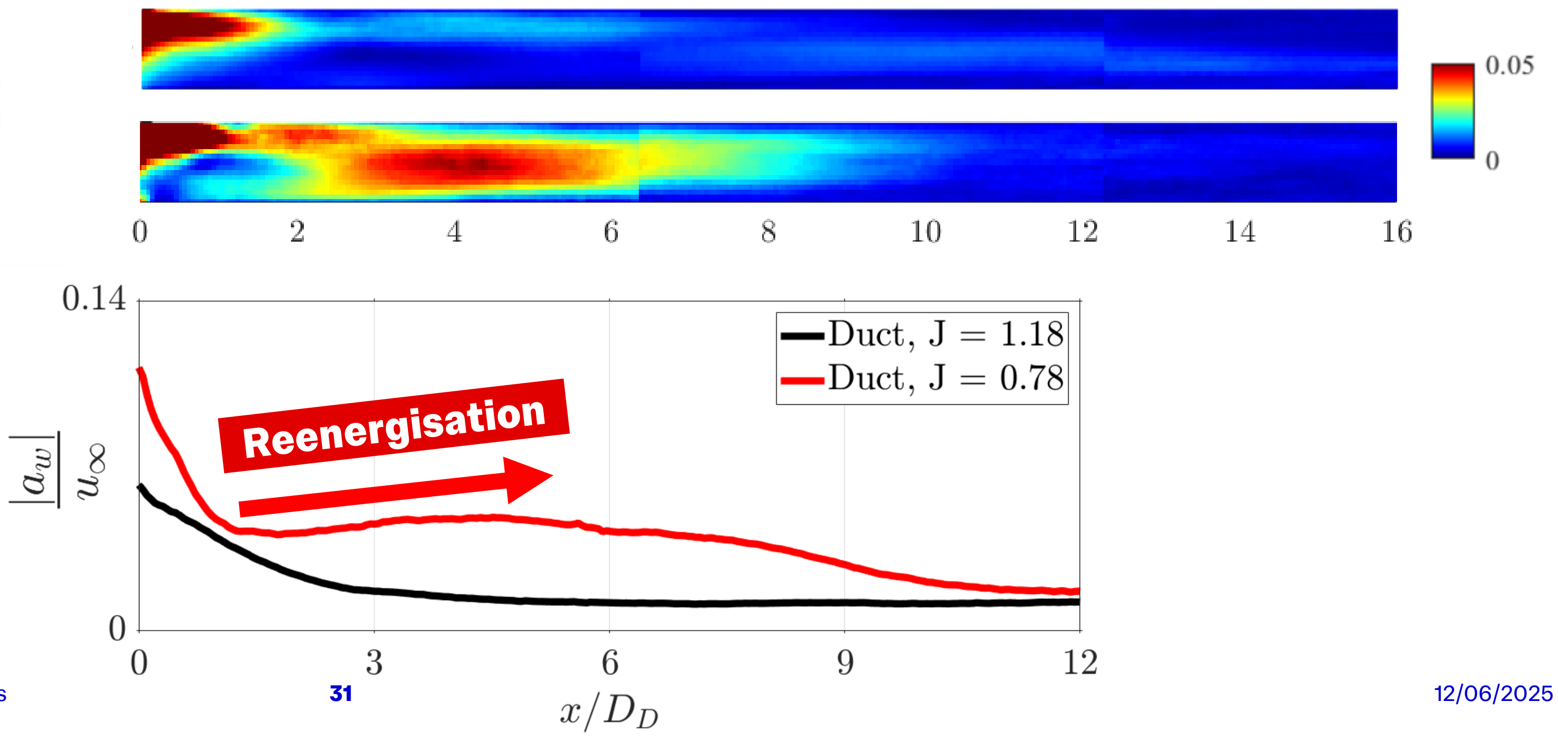

References

1) Aerospace Technology Institute. (n.d.). FlyZero. [online] Available at: https://www.ati.org.uk/flyzero/.
2) h2elios.eu. (n.d.). Home | H2ELIOS. [online] Available at: https://h2elios.eu/home.
3) ZeroAvia (2025). ZeroAvia. [online] ZeroAvia. Available at: https://zeroavia.com/.
4) Pratt and Whitney. (2024). PW100/150 Engines. [online] Available at: https://www.prattwhitney.com/en/products/regional-aviation-engines/pw100-150.
5) Park, J.S., Jung, E.Y., Lee, D.H., Kim, K.M., Kim, B.S., Chang, B.M. and Cho, H. hee (2014). Effects of Unsteady Wake on Heat Transfer of Endwall Surface in Linear Cascade. Journal of Heat Transfer, [online] 136(6). doi:https://doi.org/10.1115/1.4026373.
6) Doorly, D.J. (1988). Modeling the Unsteady Flow in a Turbine Rotor Passage. Journal of Turbomachinery, 110(1), pp.27–37. doi:https://doi.org/10.1115/1.3262164.
7) FELLI, M., CAMUSSI, R. and DI FELICE, F. (2011). Mechanisms of evolution of the propeller wake in the transition and far fields. Journal of Fluid Mechanics, [online] 682, pp.5–53. doi:https://doi.org/10.1017/jfm.2011.150.
8) Doligalski, T.L. and Walker, J.D.A. (1984). The boundary layer induced by a convected two-dimensional vortex. Journal of Fluid Mechanics, 139, pp.1–28. doi:https://doi.org/10.1017/s0022112084000240.
9) Bryce-Smith, T., Buxton, O.R.H., Papadakis, G. and Steiros, K. (2025). Propeller-induced unsteady flow inside a model cooling duct of a hydrogen-electric aircraft. In: 59th 3AF International Conference on Applied Aerodynamics.

Appendices

Methodology

Varying Blockage

How does an internal blockage affect the development of the flowfield?

- In reality, a cooling duct will have internal porous structures that obstruct the flow.

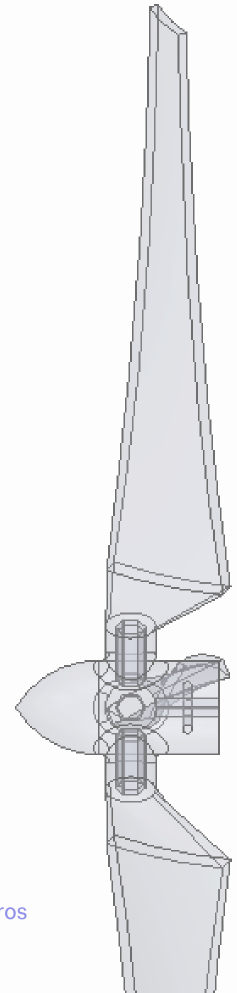

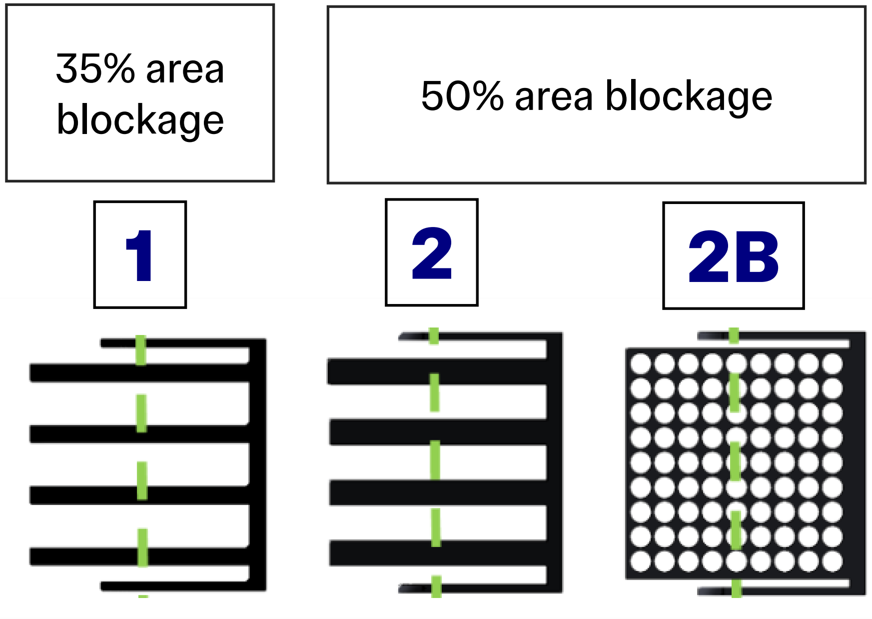

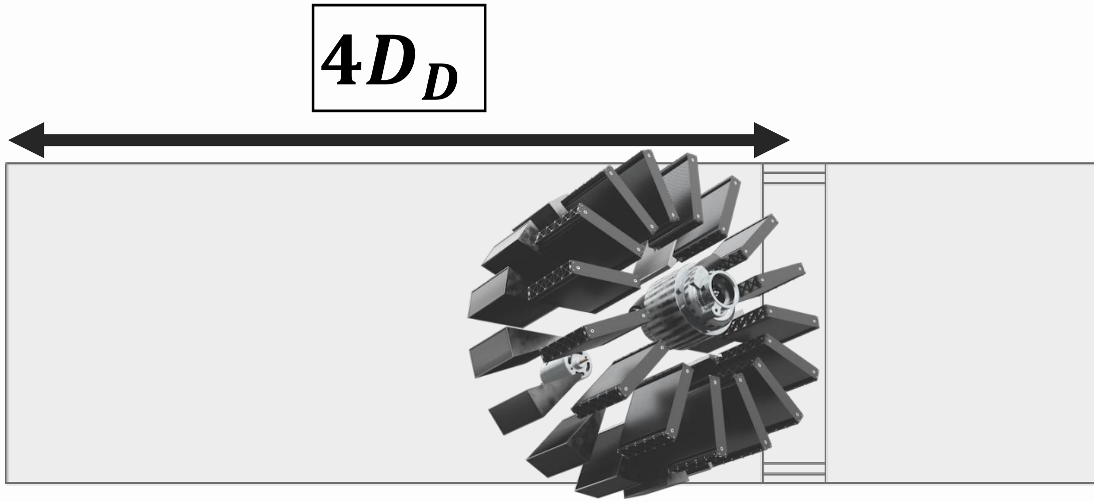

Methodology
Effect on Entrance Flow

The flow ‘feels’ the upstream obstruction, **increasing spillage** over the inlet, reducing the streamwise velocity that passes into the duct.

Mass flow rate drops within the duct by 12% and 24% for blockage 1 and 2.

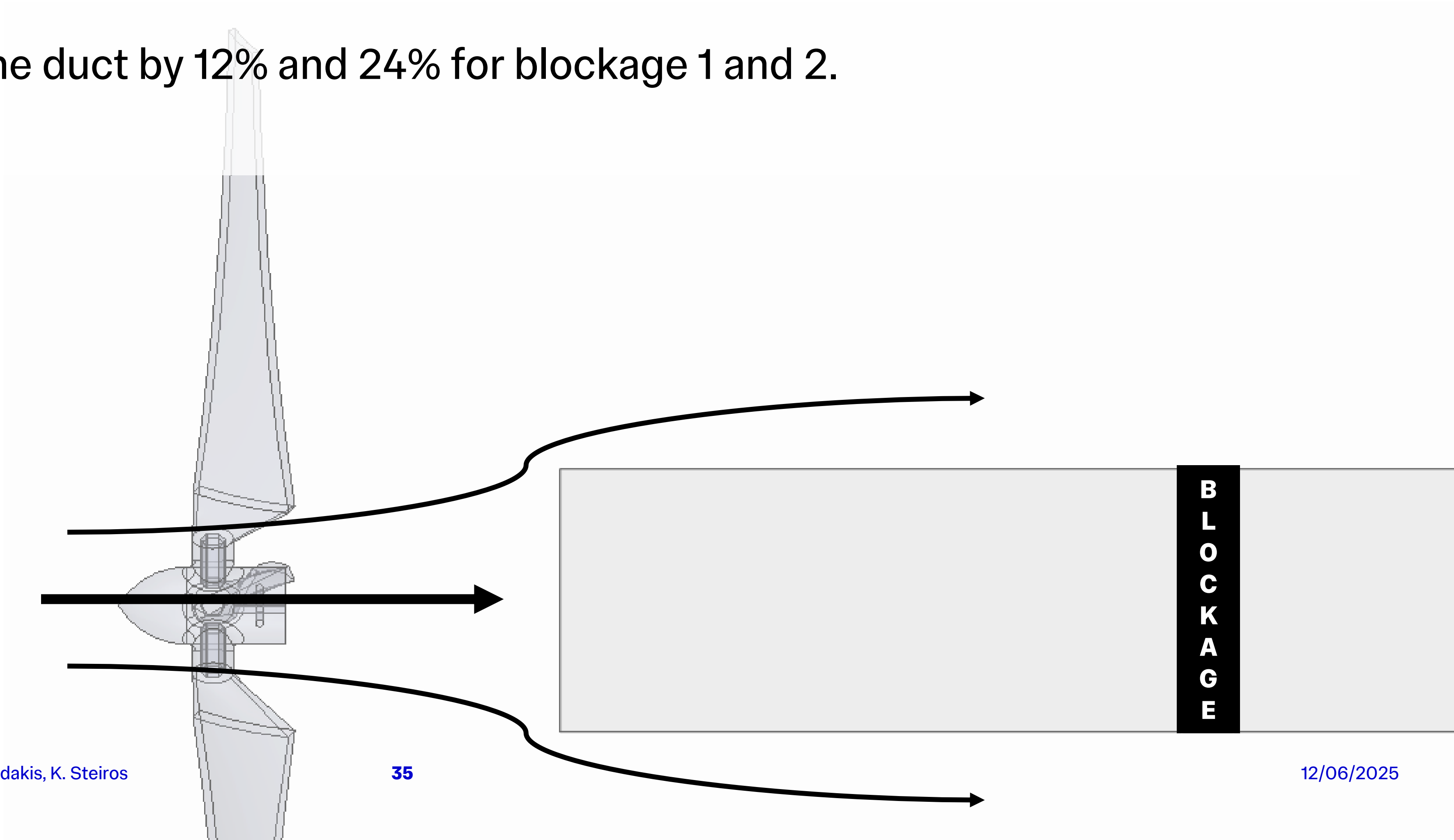

Results – Duct in Root Position with Varying Blockage

Effect on Merging

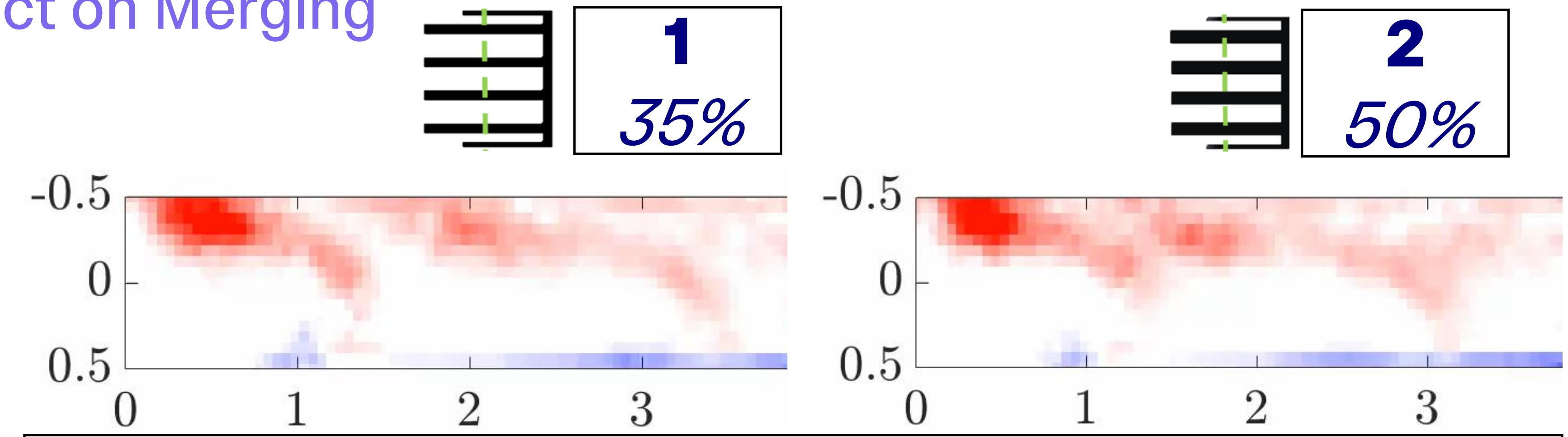

Blade wake pitch is reduced (roughly 20% in x) due to a reduced streamwise velocity as internal blockage increases

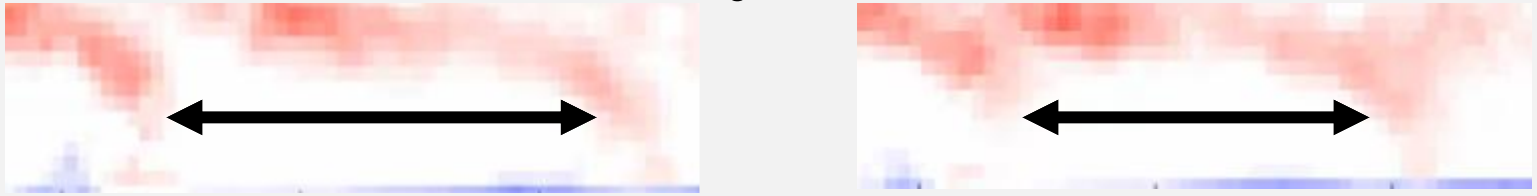

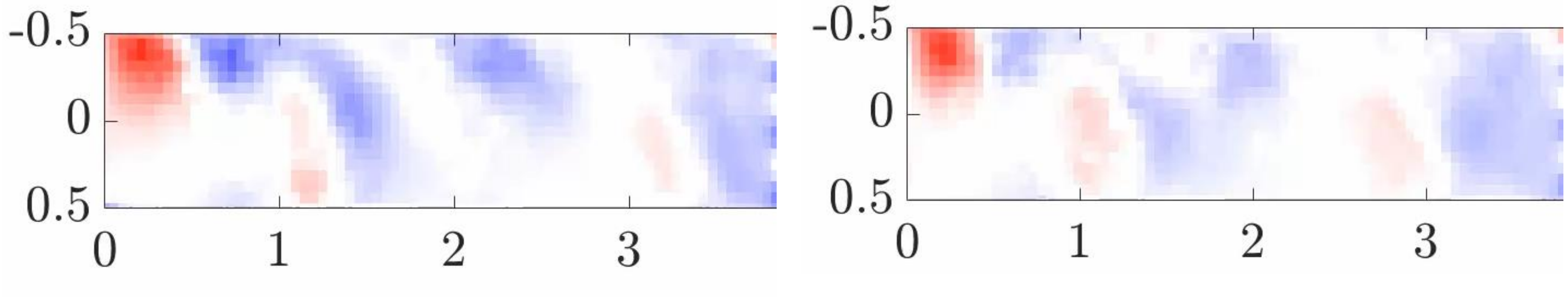

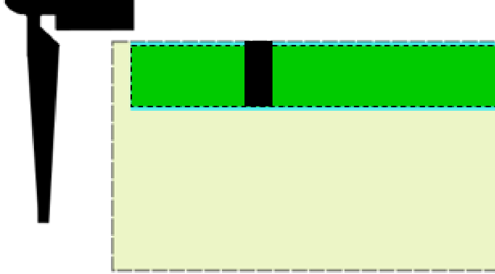

Results – Duct in Root Position with Varying Blockage

Effect on Merging

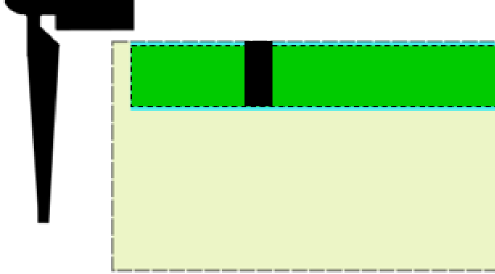

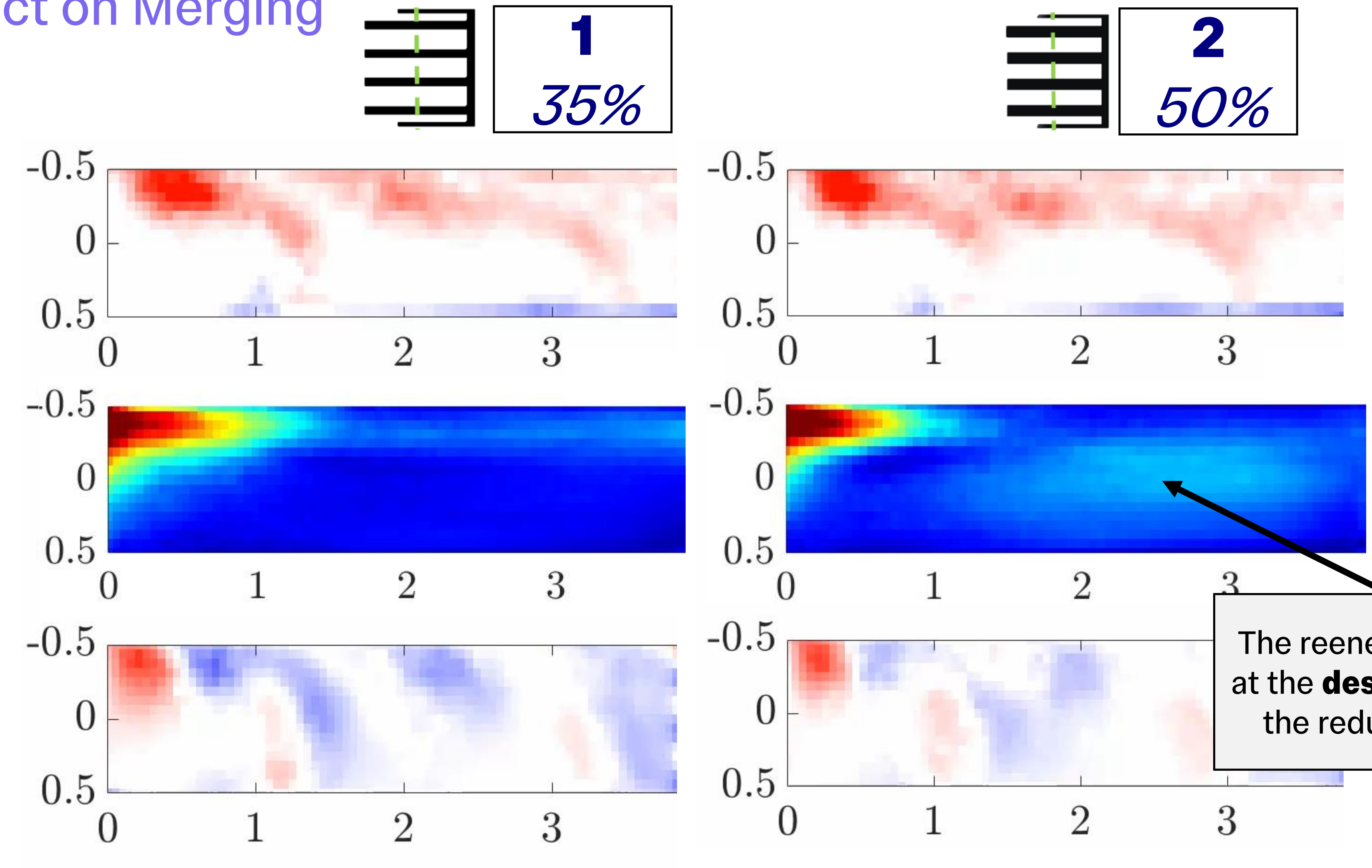

The reenergization of $3f_P$ is now seen at the **design advance ratio** owing to the reduction of blade wake pitch

Results – Duct in Root Position with Varying Blockage

Effect on Merging

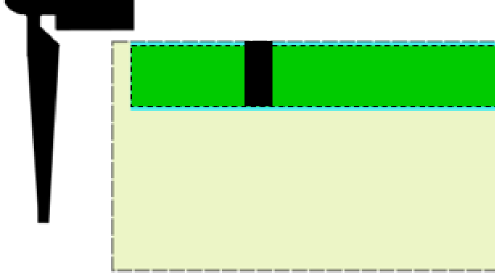

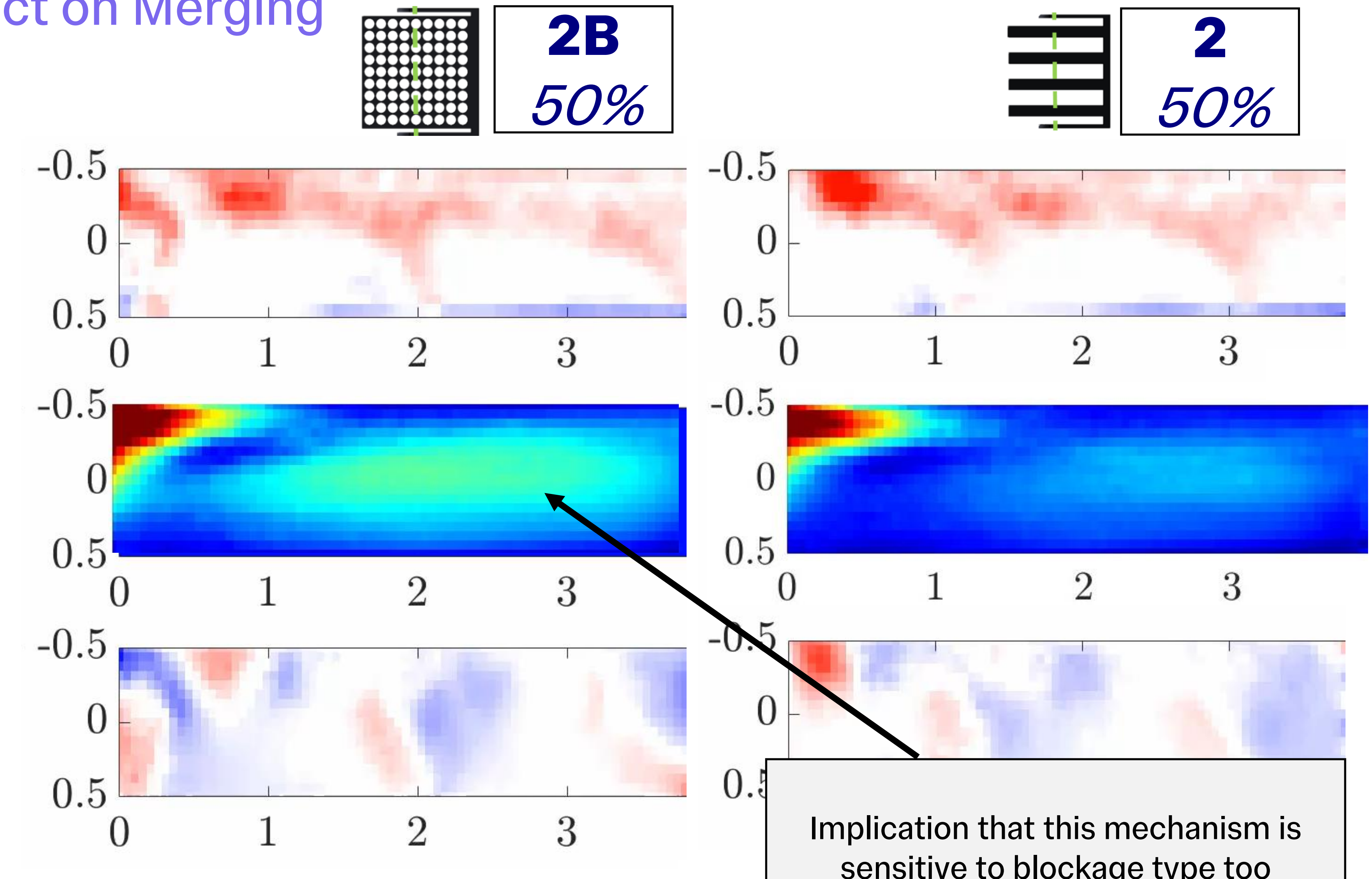

Implication that this mechanism is sensitive to blockage type too

Results – Advance Ratio vs Blockage

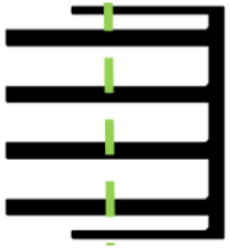

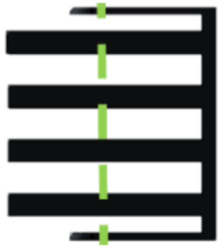

<u>Increasing Blockage</u>
- Reduces blade wake pitch
- Has a more complex relationship for the magnitude of the shear flow

As in the case of increasing propeller rotational speed, a **reenergisation of the blade passing frequency is observed**

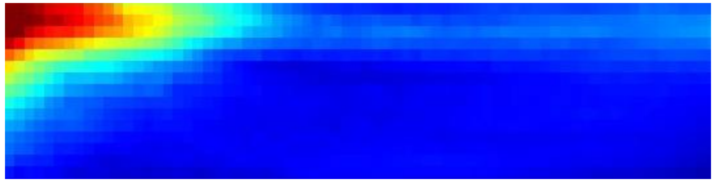

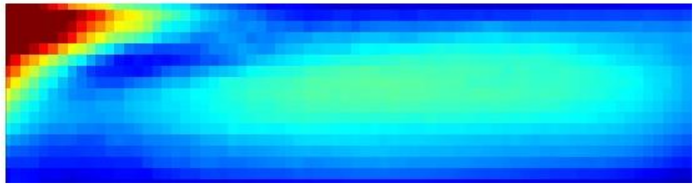

This process is also sensitive to internal blockage, via its effect on mass flow rate

Conclusions

Novel hydrogen-electric architectures suffer from **reduced cooling flux** from **lower temperature gradients** in fuel cells.

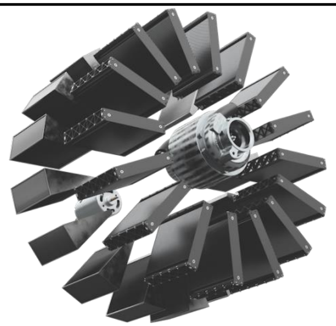

$\Delta T \approx 770°\mathrm{C}$

$\Delta T \approx 70 - 170°\mathrm{C}$

Greater coolant mass flow rate leads to a **larger drag area** ($C_D A$), **harming range and endurance** of these aircraft.

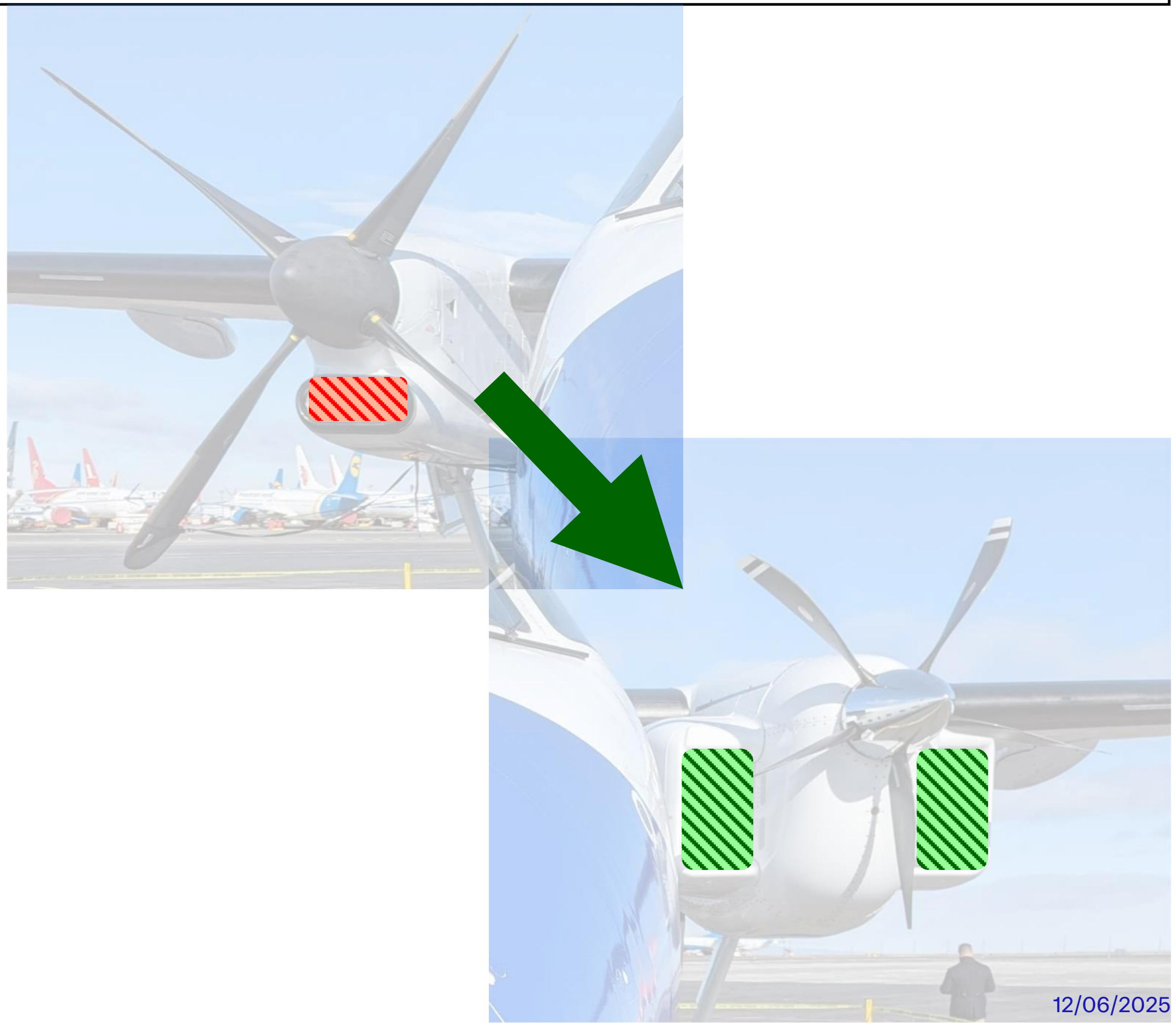

Conclusions

Novel hydrogen-electric architectures suffer from **reduced cooling flux** from **lower temperature gradients** in fuel cells.

Greater coolant mass flow rate leads to a **larger drag area** (C_DA), **harming range and endurance** of these aircraft.

Flowfield unsteadiness induced by the propeller wake brings the potential to **increase laminar heat flux** within the duct, therefore a **characterization** of an **enlarged duct immersed in propeller wake** was performed.

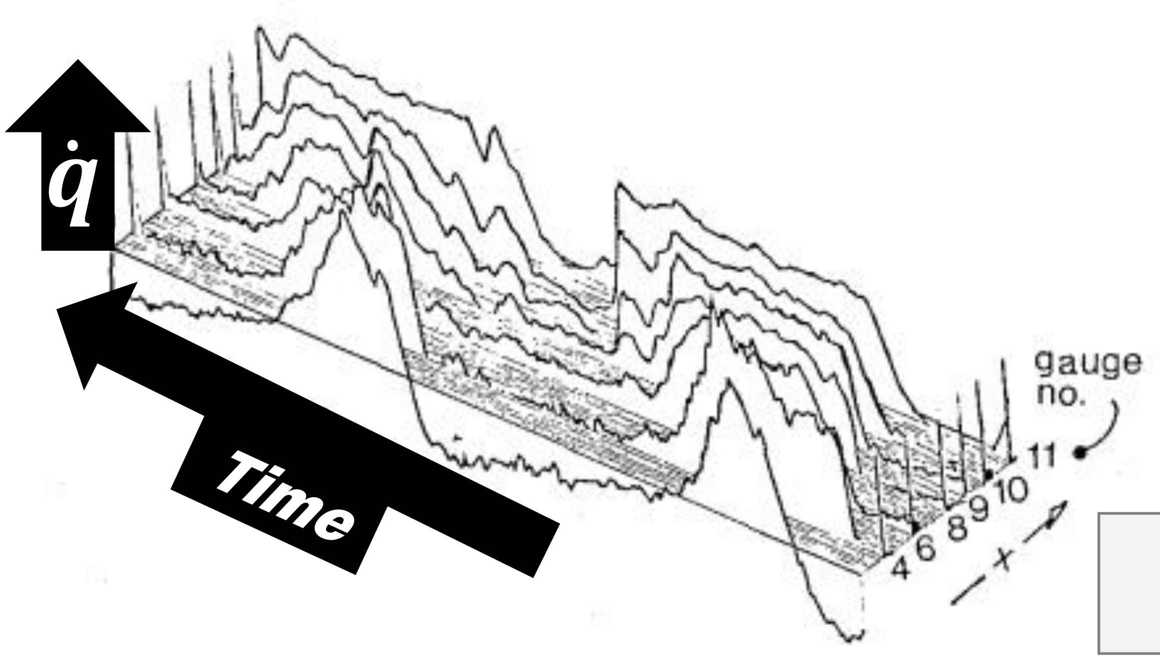

Doorly, 1988
J. Turbomachinery

Conclusions

Novel hydrogen-electric architectures suffer from **reduced cooling flux** from **lower temperature gradients** in fuel cells.

Greater coolant mas
(C_DA), **harming rang**

Flowfield unsteadiness induced by the propeller wake brings the potential to **incre**
therefore a **characterization** of an **enlarged duct immersed in prop**

A **time-resolved PIV** experiment was performed, using in-house propeller design and an optically transparent duct.

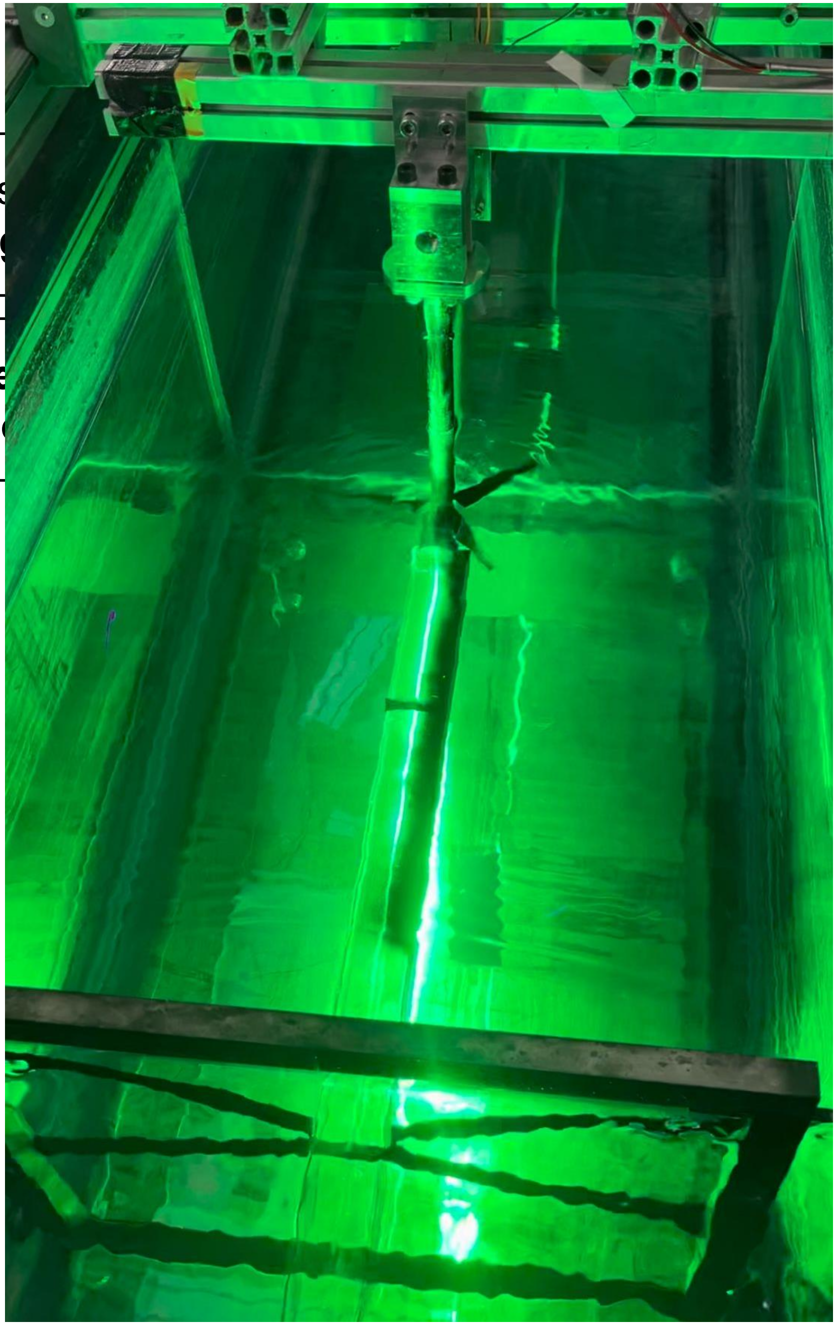

Conclusions

Novel hydrogen-electric architectures suffer from **reduced cooling flux** from **lower temperature gradients** in fuel cells.

Greater coolant mass flow rate leads to a **larger drag area** (C_DA), **harming range and endurance** of these aircraft.

Flowfield unsteadiness induced by the propeller wake brings the potential to **increase laminar heat flux** within the duct, therefore a **characterization** of an **enlarged duct immersed in propeller wake** was performed.

A **time-resolved PIV** experiment was performed, using in-house propeller design and an optically transparent duct.

Advance ratio and **internal blockage** were two varied parameters to capture industrially relevant findings.

Conclusions

Novel hydrogen-electric architectures suffer from **reduced cooling flux** from **lower temperature gradi**

Greater coolant mass flow rate leads to a **larger drag area**

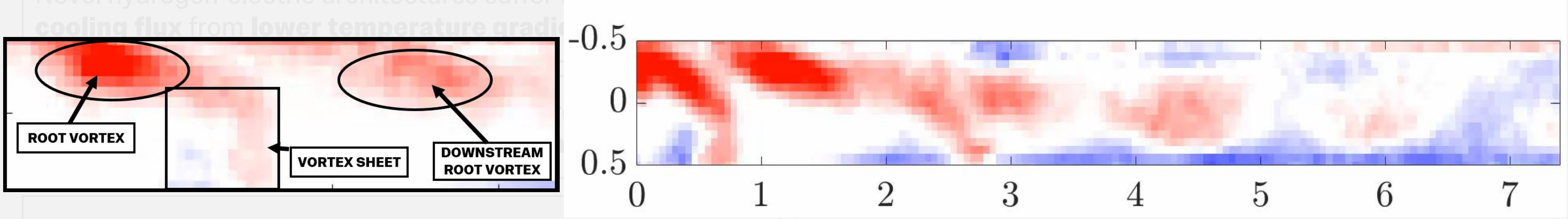

A **time-resolved PIV** experiment was performed, using in-house propeller design and an optically transparent duct.

Advance ratio and **internal blockage** were two varied parameters to capture industrially relevant findings.

The duct **ingests two discrete structures**, the root vortex and the vortex sheet, and their associated energies make the **blade passing frequency dominant** within the entrance region of the duct.

Conclusions

From Decreasing Advance Ratio

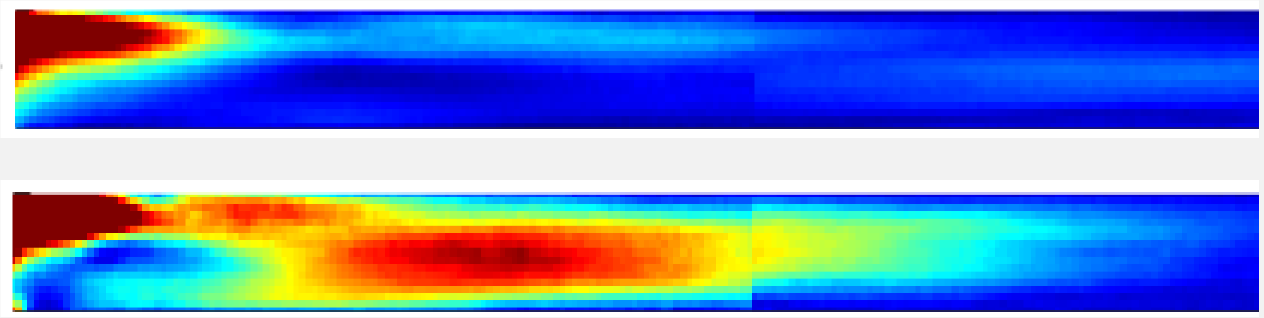

From Increasing Internal Blockage

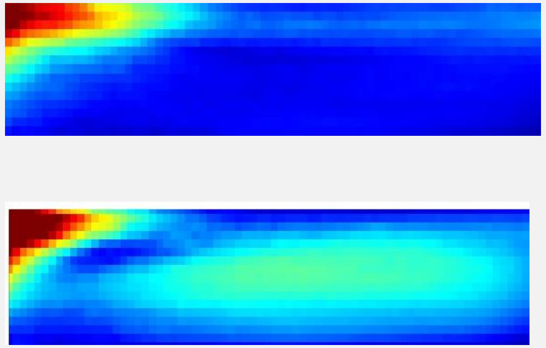

The duct **ingests two discrete structures**, the root vortex and the vortex sheet, and their associated energies make the **blade passing frequency dominant** within the entrance region of the duct.

These **structures weaken as they pass through the duct**, reducing the signature of the blade passing frequency

However, a **reenergising mechanism** is observed at the higher rotational speed and as blockage increases, from the **merging of co-rotating vortical structures.**

Conclusions

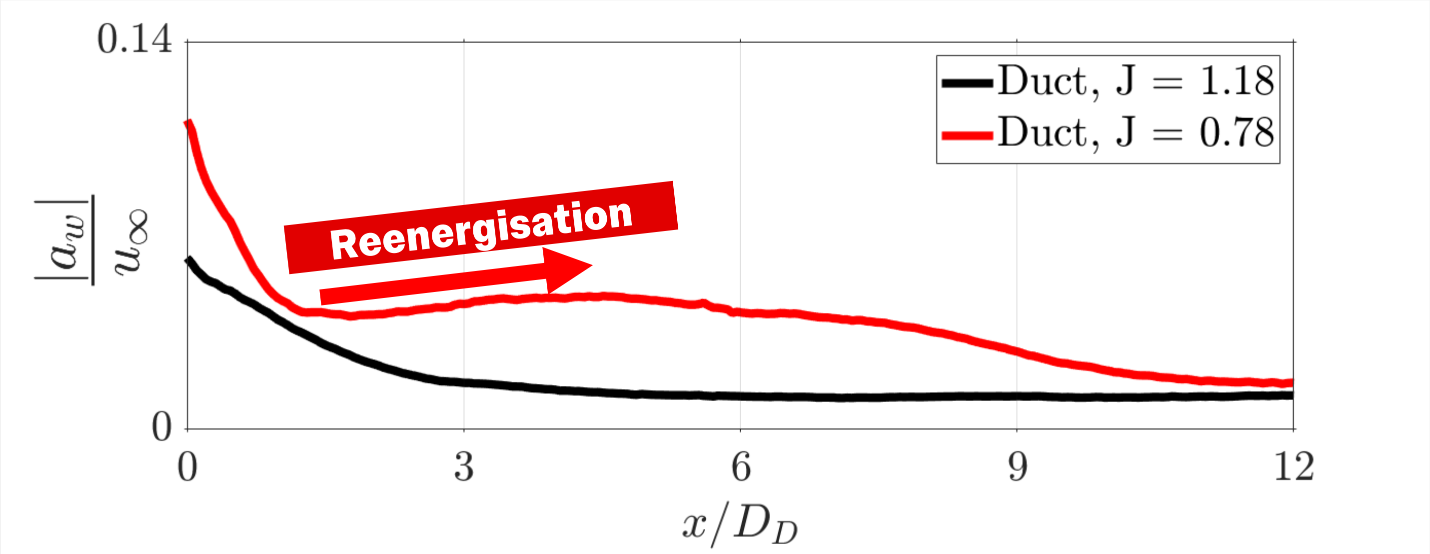

The duct **ingests two discrete structures**, the root vortex and the vortex sheet, and their associated energies make the **blade passing frequency dominant** within the entrance region of the duct.

These **structures weaken as they pass through the pipe**, reducing the signature of the blade passing frequency

However, a **reenergising mechanism** is observed at the higher rotational speed and as blockage increases, from the **merging of co-rotating vortical structures.**

This mechanism, with a deeper understanding of its activation, could enable **increased cooling flux** within hydrogen-electric powertrains, leading to a **reduced flow rate requirement** and subsequently, **reduced C_DA**.

Conclusions

Novel hydrogen-electric architectures suffer from **reduced cooling flux** from **lower temperature gradients** in fuel cells.

Greater coolant mass flow rate leads to a **larger drag area** (C_DA), **harming range and endurance** of these aircraft.

Flowfield unsteadiness induced by the propeller wake brings the potential to **increase laminar heat flux** within the duct, therefore a **characterization** of an **enlarged duct immersed in propeller wake** was performed.

A **time-resolved PIV** experiment was performed, using in-house propeller design and an optically transparent duct.

Advance ratio and **internal blockage** were two varied parameters to capture industrially relevant findings.

The duct **ingests two discrete structures**, the root vortex and the vortex sheet, and their associated energies make the **blade passing frequency dominant** within the entrance region of the duct.

These **structures weaken as they pass through the pipe**, reducing the signature of the blade passing frequency

However, a **reenergising mechanism** is observed at the higher rotational speed and as blockage increases, from the **merging of co-rotating vortical structures.**

This mechanism, with a deeper understanding of its activation, could enable **increased cooling flux** within hydrogen-electric powertrains, leading to a **reduced flow rate requirement** and subsequently, **reduced C_DA**.

IMPERIAL

Engineering and Physical Sciences Research Council

Propeller-induced Unsteady Flow Inside a Model Cooling Duct of a Hydrogen-Electric Aircraft

T. Bryce-Smith, O.R.H. Buxton, G. Papadakis, K. Steiros

Appendices

Appendix

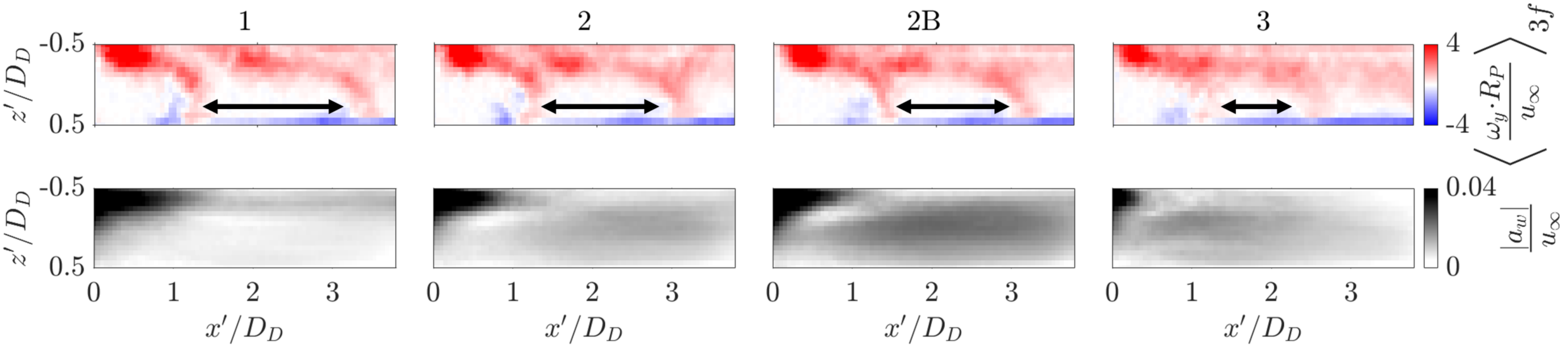

1
2
2B
3
-0.5
0.5
z'/D_D
4
-4
$\left\langle \frac{\omega_y \cdot R_P}{u_\infty} \right\rangle_{3f}$
0.04
0
$\frac{|a_w|}{u_\infty}$
0
1
2
3
x'/D_D

Appendix

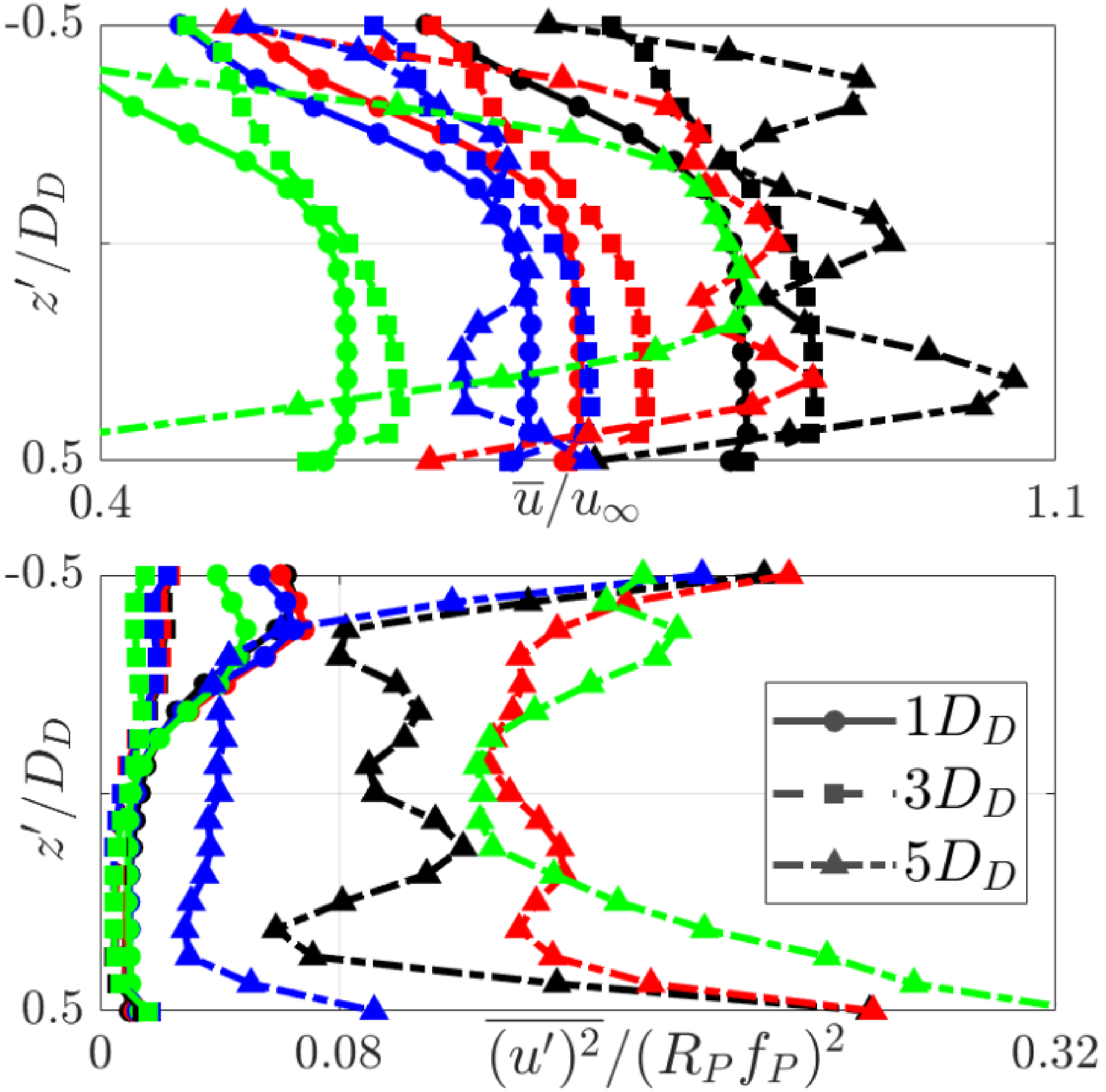

Figure 12: Mean velocity and Reynolds stressA profiles for each blockage element (1 (35%), 2 (50%), 2B (50%, holed), and 3 (65%)).

Appendix

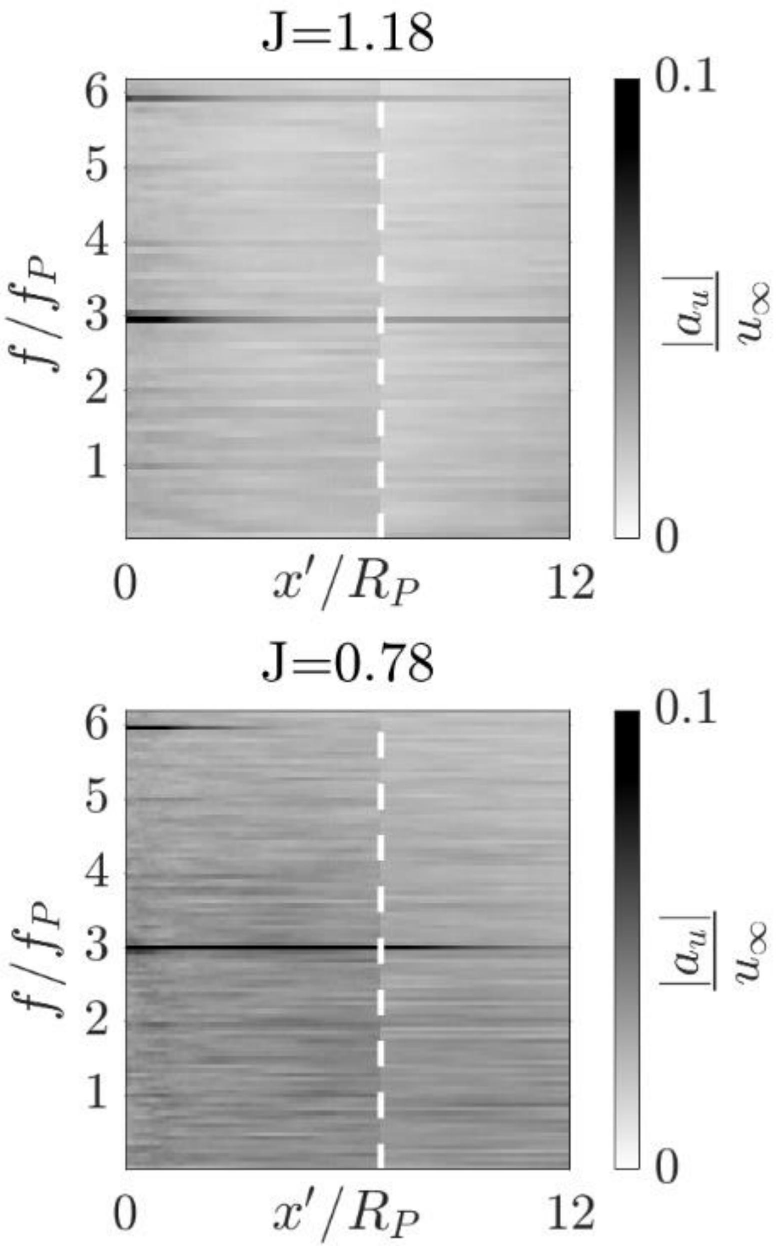

Appendix

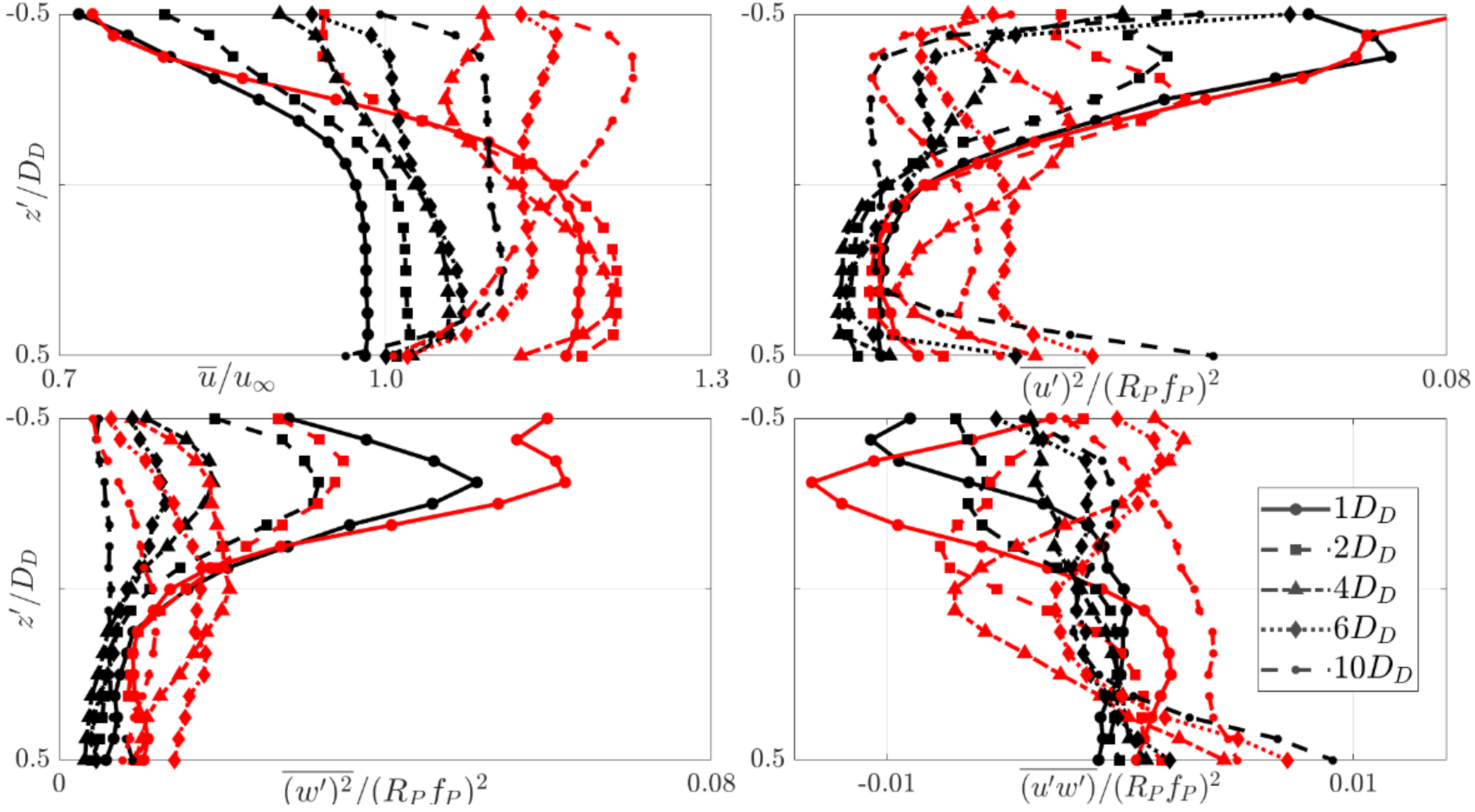

-0.5
0.5
0.7
1.0
1.3
$\overline{u}/u_\infty$
z'/D_D
0
0.08
$\overline{(u')^2}/(R_P f_P)^2$
$\overline{(w')^2}/(R_P f_P)^2$
-0.01
0.01
$\overline{(u'w')}/(R_P f_P)^2$
$1D_D$
$2D_D$
$4D_D$
$6D_D$
$10D_D$

Appendix

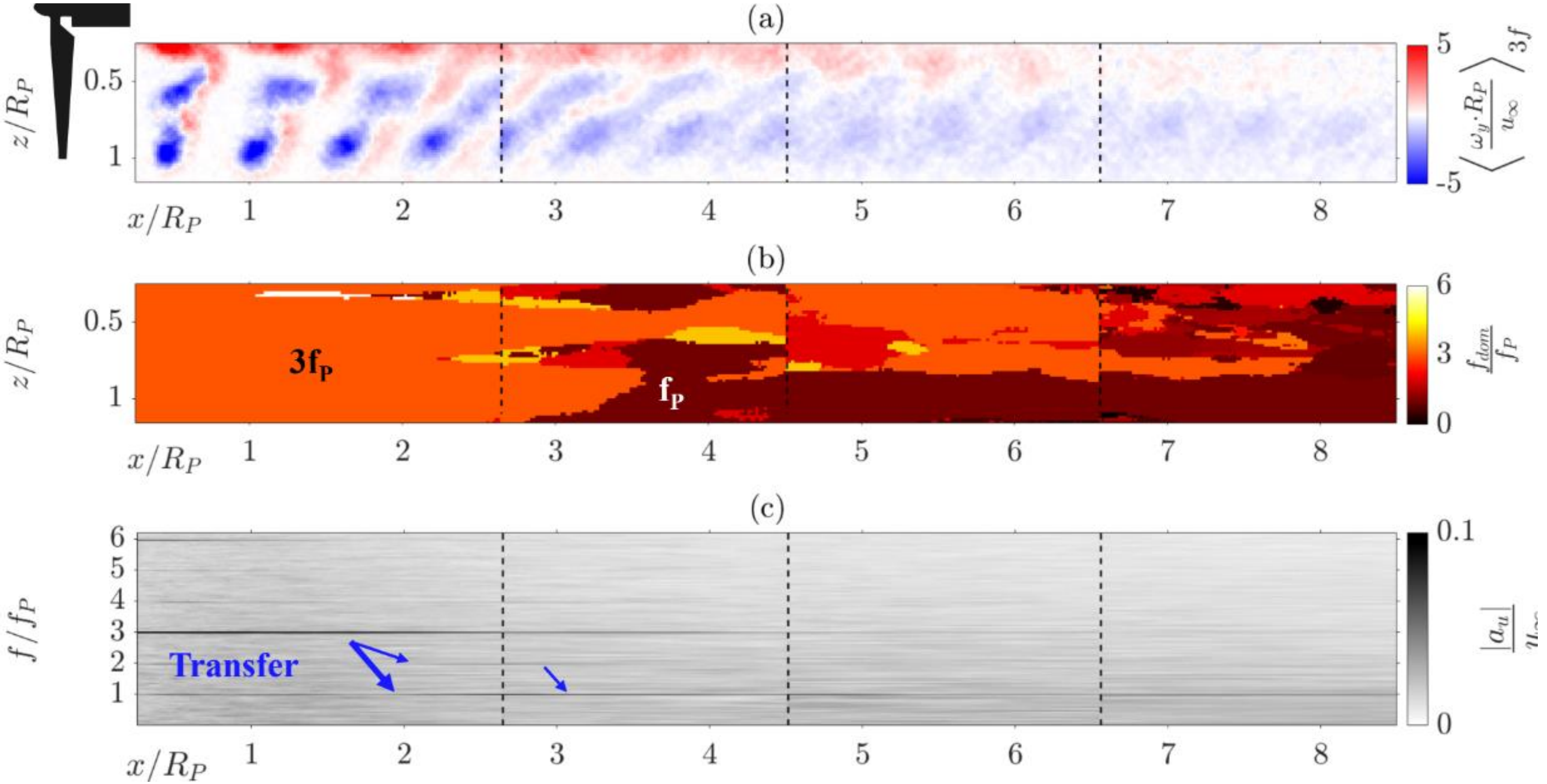

(a)
(b)
(c)
z/R_P
x/R_P
f/f_P
$3f_P$
f_P
Transfer
$\left\langle \frac{\omega_y \cdot R_P}{u_\infty} \right\rangle_{3f}$
$\frac{f_{dom}}{f_P}$
$\frac{|a_u|}{u_\infty}$

Appendix

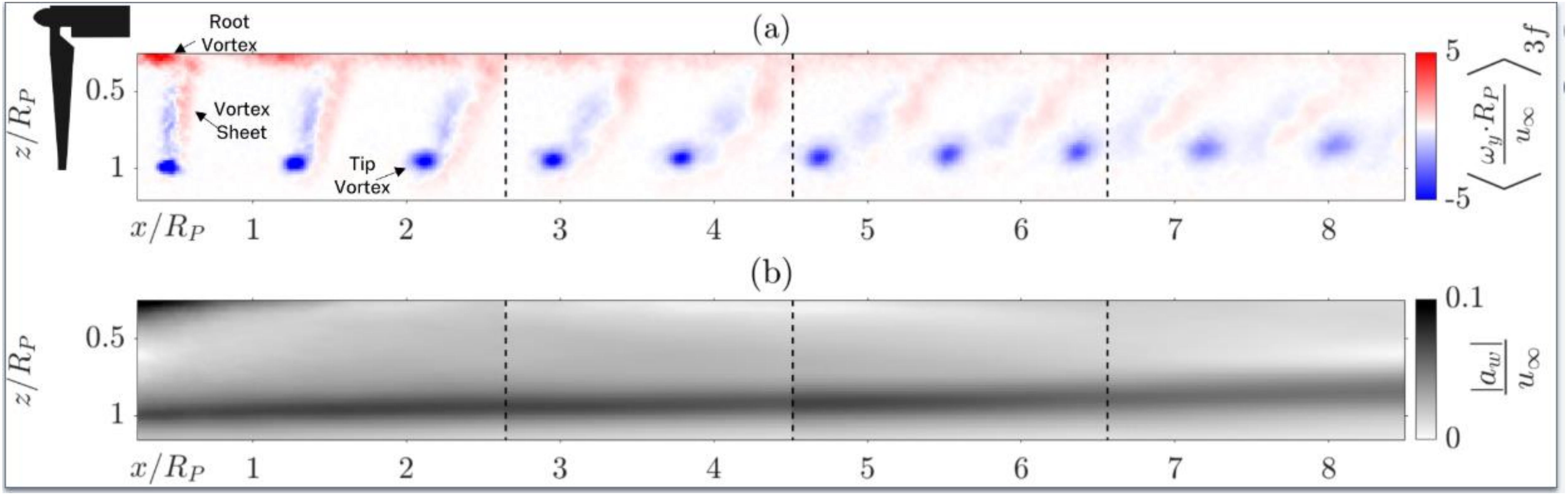
(a)
Root Vortex
Vortex Sheet
Tip Vortex
z/R_P
x/R_P
$\left\langle \frac{\omega_y \cdot R_P}{u_\infty} \right\rangle_{3f}$
(b)
z/R_P
x/R_P
$\frac{|a_w|}{u_\infty}$

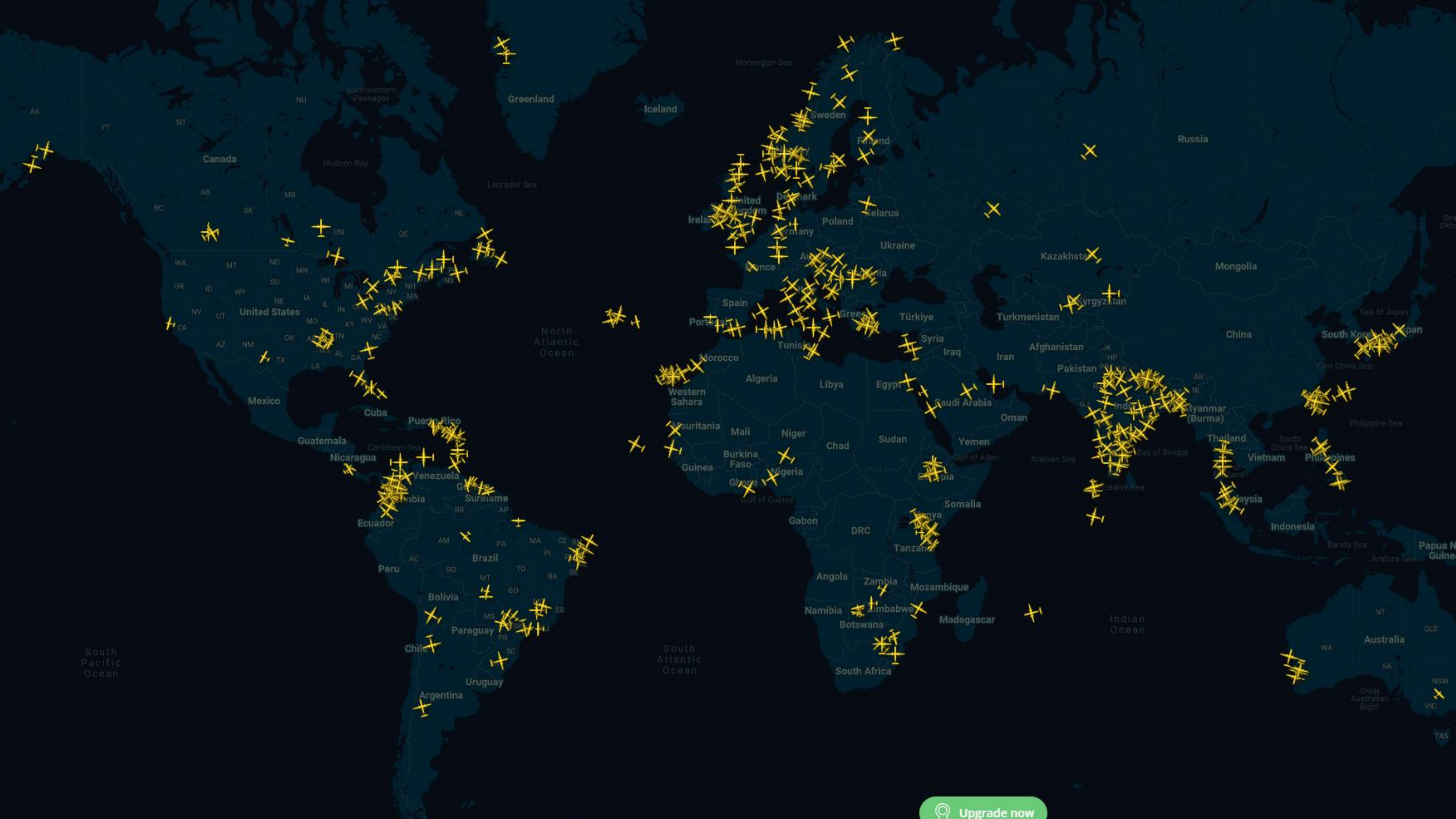

Greenland
Iceland
Norwegian Sea
Northwestern Passages
Canada
Hudson Bay
Labrador Sea
United States
Mexico
Cuba
Puerto Rico
Guatemala
Nicaragua
Caribbean Sea
Venezuela
Suriname
Ecuador
Peru
Brazil
Bolivia
Paraguay
Chile
Uruguay
Argentina
North Atlantic Ocean
South Atlantic Ocean
South Pacific Ocean
Sweden
Poland
Belarus
Ukraine
Spain
Türkiye
Morocco
Algeria
Libya
Egypt
Western Sahara
Mali
Niger
Chad
Sudan
Burkina Faso
Guinea
Nigeria
Gulf of Guinea
Gabon
DRC
Somalia
Angola
Zambia
Mozambique
Namibia
Botswana
South Africa
Madagascar
Syria
Iraq
Iran
Saudi Arabia
Oman
Yemen
Gulf of Aden
Arabian Sea
Russia
Kazakhstan
Mongolia
Turkmenistan
Afghanistan
Pakistan
China
Sea of Japan
South Korea
East China Sea
Bay of Bengal
Thailand
Vietnam
Philippine Sea
South China Sea
Indonesia
Banda Sea
Arafura Sea
Indian Ocean
Australia
Great Australian Bight
Upgrade now